SIAM J. Applied Dynamical Systems
Vol. 13, No. 3, pp. 1239–1269

A Modeling Exploration of How Synaptic Feedback to Descending Projection Neurons Shapes the Activity of an Oscillatory Network*

Nickolas Kintos† and Farzan Nadim‡

Abstract. Rhythmic activity which underlies motor output is often initiated and controlled by descending modulatory projection pathways onto central pattern generator (CPG) networks. In turn, these descending pathways receive synaptic feedback from their target CPG network, which can influence the CPG output. However, the mechanisms underlying such bidirectional synaptic interactions are mostly unexplored. We develop a reduced mathematical model, including both feed-forward and feedback circuitry, to examine how the synaptic interactions involving two projection neurons, MCN1 and CPN2, can produce and shape the activity of the gastric mill CPG in the crab stomatogastric nervous system. We use simplifying assumptions that are based on the behavior of the biological system to reduce this model down to 2 dimensions, which allows for phase plane analysis of the model output. The model shows a distinct activity for the gastric mill rhythm that is elicited when MCN1 and CPN2 are coactive compared to the rhythm elicited by MCN1 activity alone. Furthermore, the presence of feedback to the projection neuron CPN2 provides a distinct locus of pattern generation in the model which does not require reciprocally inhibitory interactions between the gastric mill CPG neurons, but is instead based on a half-center oscillator that occurs through a trisynaptic pathway that includes CPN2. Our modeling results show that feedback to projection pathways may provide additional mechanisms for the generation of motor activity. These mechanisms can have distinct dependence on network parameters and may therefore provide additional flexibility for the rhythmic motor output.

Key words. limit cycle, forced oscillation, phase plane, neuromodulation, stomatogastric, neural oscillation

AMS subject classifications. 92C20, 34A26, 37C27

DOI. 10.1137/130943881

1. Introduction.

Projection neuron pathways play an important role in generating and shaping the activity patterns of neural networks. In mammals, for example, descending projection pathways from the cerebellum and brainstem influence the rhythmic networks that generate locomotor activity in the spinal cord [30, 44, 12]. The influence of projection pathways on neural networks is typically studied assuming a feed-forward architecture, in which descending projection neuron pathways initiate, terminate, or modify the activity of the target network [7, 21, 39, 15]. However, neural circuitry in biological systems is more complex, in that projection neurons receive feedback from their target networks [8, 38, 34, 45]. In rhythmically active oscillatory networks, such feedback can influence the pattern of descending inputs from projection neurons, and, in some cases, rhythmically patterned projection neuron

*Received by the editors November 4, 2013; accepted for publication (in revised form) by B. Ermentrout May 6, 2014; published electronically August 12, 2014. This research was supported by NIH MH060605 (FN) and the Kenny Fund Fellowship (NK).
http://www.siam.org/journals/siads/13-3/94388.html
†Department of Mathematics, Saint Peter's University, Jersey City, NJ 07306 (nkintos@saintpeters.edu).
‡Corresponding author. Department of Biological Sciences and Department of Mathematical Sciences, New Jersey Institute of Technology, Newark, NJ 07102 (farzan@njit.edu).

input influences the motor pattern of the target network [42]. However, in most systems, the consequences of patterned projection neuron input are generally unknown for the activity of the target networks.

We investigate the role of feedback to projection neurons in a mathematical model of the crab gastric mill network [36]. The gastric mill network is located within the stomatogastric ganglion (STG), one of the four main ganglia of the stomatogastric nervous system (STNS). The neural circuitry within the STG is innervated by descending inputs from ∼20 pairs of descending projection neurons whose cell bodies are located within the anterior ganglia of the STNS [36]. Within the STG gastric mill neural circuit, interneuron 1 (Int1) and the lateral gastric (LG) neuron reciprocally inhibit each other and form an asymmetric, half-center oscillator, which underlies the activity of the gastric mill rhythm [14, 32]. The gastric mill rhythm is generally not spontaneously active [3, 5]. However, tonic stimulation of the identified projection neuron modulatory commissural neuron 1 (MCN1) readily elicits a gastric mill rhythm (frequency ∼0.1 Hz) in vitro. Moreover, within the STG, modulatory synaptic input from MCN1 axon terminals and presynaptic inhibition of those terminals by the LG neuron are necessary for MCN1 to activate the gastric mill rhythm [14]. The gastric mill network receives synaptic input from the faster (∼1 Hz) pyloric rhythmic network in the form of synaptic inhibition from the pyloric pacemaker AB neuron to Int1. This fast rhythmic input has a strong influence on the cycle frequency of the MCN1-elicited gastric mill rhythm [3, 32].

The MCN1 soma is located in the commissural ganglia (CoGs; a pair of anterior STNS ganglia located several centimeters away from the STG) and is often coactive with a second CoG projection neuron, the commissural projection neuron 2 (CPN2), to elicit a version of the gastric mill rhythm that is distinct from the MCN1-elicited rhythm [5]. CPN2 axon terminals excite the LG neuron within the STG [34], and this excitation may be partly due to an electrical coupling [35]. Both projection neurons, MCN1 and CPN2, receive rhythmic feedback from the STG neurons in the biological system [10, 34, 43]. In particular, CPN2 is inhibited by Int1 via a feedback synapse in the CoGs [34].

We previously used modeling to explore the mechanisms underlying the MCN1-elicited gastric mill rhythm [26, 2, 32]. We now develop a mathematical model to investigate how the distinct gastric mill rhythm which is elicited by coactivation of MCN1 and CPN2 (the MCN1+CPN2-elicited gastric mill rhythm) is influenced by the interplay of synaptic connections between CPN2 and the gastric mill CPG neurons. Physiologically, our model is motivated by the gastric mill rhythm that is elicited by MCN1 and CPN2 when they are coactivated by the ventral cardiac neurons (VCNs) [5]. However, in this study we focus only on the influence of gastric mill rhythmic feedback to CPN2, and MCN1 is assumed to be tonically active in our model. This enables us to directly compare our results for the MCN1+CPN2-elicited gastric mill rhythm with the gastric mill motor pattern of the MCN1-elicited rhythm from previous experiments [14, 3] and modeling [32, 26]. The general properties of the MCN1+CPN2-elicited gastric mill rhythm in our model remain similar to those of the VCN-elicited rhythm in the biological system.

Our model builds upon our previous mathematical model of the MCN1-elicited gastric mill rhythm [26]. In the current model, we ignore the intrinsic properties of CPN2 and simply focus on the question of how the synaptic interactions of this projection neuron influence the

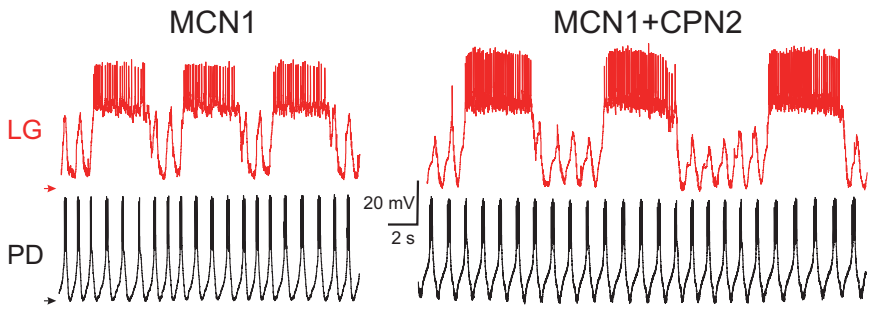

Figure 1. *The gastric mill rhythm in the biological system. Coactivation of the projection neurons MCN*1 *and CPN*2 *(right) elicits a distinct and slower version of the gastric mill rhythm from that which is produced by MCN*1 *activity alone (left). The activity of the PD neuron (shown in black) represents the pyloric rhythm, whose frequency is an order of magnitude faster than that of the gastric mill rhythm. The influence of the pyloric rhythm on the gastric mill rhythm is seen in the subthreshold depolarizations in the LG neuron between its rhythmic bursts. Arrows indicate* -60 *mV. (Data recorded by FN.)*

gastric mill rhythm. Our focus on synaptic interactions leads us to a reduced 2-dimensional model of the MCN1+CPN2-elicited gastric mill rhythm which allows for a phase plane analysis of the network dynamics. Moreover, this simplified model allows for a comparison of CPN2 excitatory input on the network dynamics through a chemical synapse versus CPN2 excitation through electrical coupling. The results of our simplified model demonstrate that coactivation of the two projection neurons plus feedback from the target network allows for (i) a different range of oscillation frequencies in the target network, and (ii) the appearance of a distinct locus of pattern generation in the target network. Additionally, we show that a weaker MCN1 input has a similar influence on distinct circuit configurations that produce the MCN1+CPN2-elicited gastric mill rhythm in the model.

2. Methods.

The mathematical model of the MCN1+CPN2-elicited gastric mill rhythm builds on our previously published, reduced 3-dimensional model of the MCN1-elicited gastric mill rhythm, which showed that the synaptic circuitry underlying this rhythm can produce the proper network dynamics. A reduction of this model down to 2 dimensions, using the difference in synaptic time scales exhibited in the biological system, allowed for the analysis of the network dynamics of the MCN1-elicited gastric mill rhythm using the geometric properties within a 2-dimensional phase plane [26].

Here, we also construct a 2-dimensional mathematical model, but of the MCN1+CPN2-elicited gastric mill rhythm. Physiologically, coactivation of MCN1 and CPN2 activates a different version of the gastric mill rhythm than MCN1 stimulation alone [5] (Figure 1). Despite the differences between these two versions, in both cases, the reciprocally inhibitory CPG neurons, Int1 and LG, comprise a half-center oscillator which underlies the generation of the gastric mill rhythmic activity. Our model here accounts only for the slow envelope of network oscillations in order to simplify the network interactions for our mathematical analysis. Thus, we ignore action potentials and action-potential mediated synaptic transmission in the model neurons. Physiologically, STG neurons operate with a strong component of graded synaptic transmission [27], and here we consider only the graded component of synaptic transmission between the neurons in our model. Finally, because of our focus on the network mechanisms,

we will ignore voltage-gated ionic currents and treat Int1 and LG as passive neurons [28].

2.1. A 4-dimensional model of the MCN1+CPN2-elicited gastric mill rhythm. Our mathematical model of the MCN1+CPN2-elicited gastric mill rhythm begins with a system of 4 nonlinear differential equations, given by

(1)
$$C_I \frac{dV_I}{dt} = -\underbrace{g_{Leak,I}\,(V_I - E_{Leak,I})}_{I_{Leak,I}} - \underbrace{\bar{g}_{L\to I} m_{L\to I}\,(V_L)\,(V_I - E_{L\to I})}_{I_{L\to I}} - \underbrace{\bar{g}_P P\,(t, V_L)\,(V_I - E_P)}_{I_P},$$

(2)
$$C_L \frac{dV_L}{dt} = -\underbrace{g_{Leak,L}\,(V_L - E_{Leak,L})}_{I_{Leak,L}} - \underbrace{\bar{g}_{I\to L} m_{I\to L}\,(V_I)\,(V_L - E_{I\to L})}_{I_{I\to L}} - \underbrace{\bar{g}_s s\,(V_L - E_s)}_{I_s}$$
$$- \underbrace{\bar{g}_{C\to L} m_{C\to L}\,(V_C)\,(V_L - E_{C\to L})}_{I_{C\to L}} - \underbrace{g_{elec}\,(V_L - V_C)}_{I_{elec}},$$

(3)
$$C_C \frac{dV_C}{dt} = -\underbrace{g_{Leak,C}\,(V_C - E_{Leak,C})}_{I_{Leak,C}} - \underbrace{\bar{g}_{I\to C} m_{I\to C}\,(V_I)\,(V_C - E_{I\to C})}_{I_{I\to C}},$$

(4)
$$\frac{ds}{dt} = \begin{cases} \dfrac{1-s}{\tau_{LO}}, & V_L \le v_{thresh}, \\ \dfrac{-s}{\tau_{HI}}, & V_L > v_{thresh}. \end{cases}$$

Equations (1)–(4) describe the evolution of the four state variables in the model: the membrane potentials of Int1 (V_I), the LG neuron (V_L), and CPN2 (V_C), and the slow excitatory input (s) from MCN1 to LG (Figure 2(A)). On the left-hand side of (1)–(3), the parameters C_I, C_L, and C_C represent the membrane capacitance of Int1, the LG neuron, and CPN2, respectively. We set these to 1 for simplicity.

On the right-hand side of (1)–(2), the terms $I_{Leak,I}$ and $I_{Leak,L}$ represent the leak current in Int1 and the LG neuron, respectively, with $g_{Leak,I}$ and $E_{Leak,I}$ ($g_{Leak,L}$ and $E_{Leak,L}$) representing the leak conductance and reversal potential of Int1 (LG). In the biological system, the excitatory synaptic input s from MCN1 is necessary to elicit a gastric mill rhythm [14]. Without the input from MCN1, Int1 exhibits a high membrane potential and remains active, while the LG neuron exhibits a low membrane potential and remains inactive [3]. As in previous work [26], we produce this asymmetry between Int1 and the LG neuron by assigning a high value to $E_{Leak,I}$ and a low value to $E_{Leak,L}$ in our model (see Table 1).

The term $I_{Leak,C}$ on the right-hand side of (3) models the leak current in CPN2, with $g_{Leak,C}$ and $E_{Leak,C}$ representing the leak conductance and reversal potential, respectively. We assign a high value to $E_{Leak,C}$, indicating that CPN2 remains active whenever it is not inhibited by Int1.

The terms $I_{L\to I}$ and $I_{I\to L}$ in (1)–(2) describe the reciprocally inhibitory synapses between Int1 and the LG neuron. Similarly $I_{I\to C}$ on the right-hand side of (3) models the inhibitory

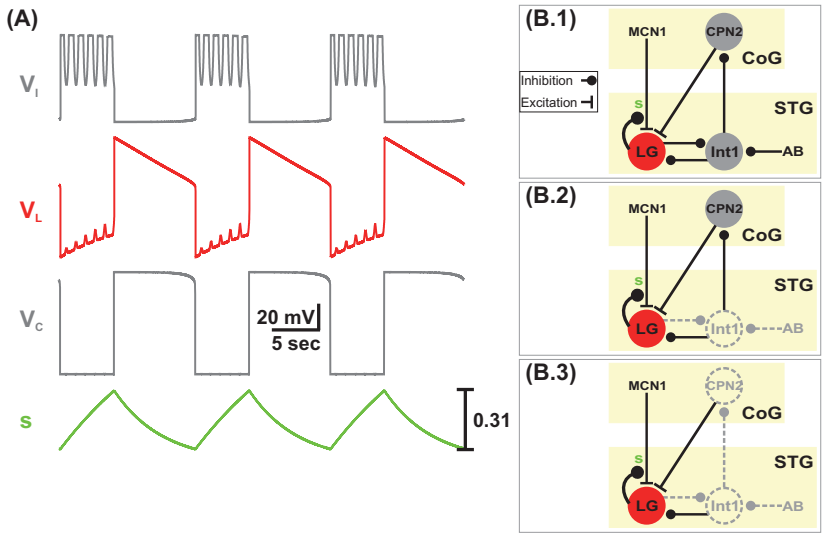

Figure 2. *Output of the mathematical model of the gastric mill CPG.* (A) *The time course of all state variables in the* 4*-dimensional model (eqs.* (1)–(4)*).* (B.1) *Circuit diagram of the* 4*-dimensional model. AB and MCN*1 *are not modeled explicitly but only through their postsynaptic influences. The projection neurons MCN*1 *and CPN*2 *are in the CoG and spatially separated from the gastric mill network (in the STG). The LG neuron and Int*1 *reciprocally inhibit each other, and Int*1 *is inhibited by a pyloric-timed synaptic input from AB, the pacemaker of the pyloric circuit. The LG neuron receives excitatory synaptic input from both projection neurons (MCN*1 *and CPN*2*), and it presynaptically inhibits MCN*1 *within the STG. In the CoG, CPN*2 *is inhibited by a feedback synapse from Int*1*.* (B.2) *Circuit diagram of the reduced* 3*-dimensional model (eqs.* (11)–(13)*). Due to the difference in time scales,* V_I *can be expressed in terms of* V_L *(the effects of Int*1 *and AB are absorbed into the* V_L *equation). The activity of* V_L*,* V_C*, and* s *remains practically identical to that of the* 4*-dimensional model shown in* (A)*.* (B.3) *Circuit diagram of the reduced* 2*-dimensional model (eqs.* (16)–(17)*).* V_C *can be expressed in terms of* V_L *(the effect of CPN*2 *is absorbed into the* V_L *equation). The activity of* V_L *and* s *remains practically identical to the traces in* (A)*.*

Table 1

Parameter values for the reduced 2*-dimensional model of the MCN*1*+CPN*2*-elicited gastric mill rhythm.*

Int1	**AB** (P)	**CPN2**	**LG**	**MCN1** (s)
$g_{Leak,I} = 0.75$ mS/cm^2	$\bar{g}_P = 0.85$ mS/cm^2	$g_{Leak,C} = 1$ mS/cm^2	$g_{Leak,L} = 1$ mS/cm^2	$\bar{g}_s = 7.5$ mS/cm^2
$E_{Leak,I} = 10$ mV	$E_P = -60$ mV	$E_{Leak,C} = 10$ mV	$E_{Leak,L} = -60$ mV	$E_s = 50$ mV
$\bar{g}_{L\to I} = 2$ mS/cm^2	$per = 1$ sec	$\bar{g}_{I\to C} = 17$ mS/cm^2	$\bar{g}_{I\to L} = 12$ mS/cm^2	$v_{thresh} = -27$ mV
$E_{L\to I} = -80$ mV	$dur = 0.5$ sec	$E_{I\to C} = -80$ mV	$E_{I\to L} = -80$ mV	$\tau_{LO} = 14$ sec
$v_{L\to I} = -30$ mV	$v_q = -35$ mV	$v_{I\to C} = -40$ mV	$v_{I\to L} = -30$ mV	$\tau_{HI} = 5$ sec
$k_{L\to I} = 5$ mV	$k_q = 3$ mV	$k_{I\to C} = 3$ mV	$k_{I\to L} = 5$ mV	
$C_I = 1\ \mu$F/cm^2		$C_C = 1\ \mu$F/cm^2	$\bar{g}_{C\to L} = 0.5$ mS/cm^2	
$\tau_I = 0.0013\bar{3}$ sec		$\tau_C = 0.001$ sec	$E_{C\to L} = 30$ mV	
			$v_{C\to L} = -25$ mV	
			$k_{C\to L} = 8$ mV	
			$g_{elec} = 0.7$ mS/cm^2	
			$C_L = 1\ \mu$F/cm^2	
			$\tau_L = 0.001$ sec	

feedback synapse from Int1 onto the CPN2 soma in the CoG (Figure 2(B.1)). The parameters $\bar{g}_{pre\to post}$ and $E_{pre\to post}$ represent the synaptic maximal conductance and reversal potential of these synapses. The synapses are gated by functions $m_{pre\to post}(V_{pre})$ which depend on the membrane potential of the presynaptic neuron and are modeled as a sigmoid:

$$m_{pre\to post}\left(V_{pre}\right) = \frac{1}{1+\exp\left(\left(v_{pre\to post}-V_{pre}\right)/k_{pre\to post}\right)}. \tag{5}$$

The parameters $v_{pre\to post}$ and $k_{pre\to post}$ in (5) describe the half-activation voltage and steepness of the sigmoid.

The term I_P on the right-hand side of (1) models the inhibitory synapse from the pyloric pacemaker AB neuron onto Int1 within the STG (Figure 2(B.1)), with $\bar{g}_P$ and E_P representing its maximal conductance and reversal potential, respectively. This synapse is gated by the function $P(t, V_L)$, and, to show the separate time- and voltage-dependent components, we can rewrite the gating function as

$$P\left(t, V_L\right) = P\left(t\right) q\left(V_L\right). \tag{6}$$

This synaptic input essentially acts as a periodic forcing input to the gastric mill network and, here, the time-dependent component is modeled as a periodic, half-sine function

$$P\left(t\right) = \sin\left(\frac{\pi \bmod\left(t, per\right)}{dur}\right) H\left(dur - \bmod\left(t, per\right)\right), \tag{7}$$

where mod() and $H()$ designate the modulo and Heaviside function, respectively. The parameters *per* and *dur* represent the period and duty cycle, respectively, of this half-sine function. As mentioned above, the pyloric rhythm cycle frequency (∼1 Hz) is an order of magnitude faster than the gastric mill rhythm (∼0.1 Hz) [3]. We account for this by assigning appropriate values to the parameters *per* and *dur* in our model (see Table 1).

The voltage-dependent component of the gating function in (6) is given by the decreasing sigmoid

$$q\left(V_L\right) = \frac{1}{1+\exp\left(\left(V_L - v_q\right)/k_q\right)}, \tag{8}$$

where v_q and k_q describe its half-activation voltage and steepness, respectively. We have included this voltage-dependent component in the gating function in order to account for the fact that the AB to Int1 synapse is gated out during the active phase of the LG neuron in the gastric mill cycle [3]. This gating is incorporated into our model by (8), which turns off the pyloric-timed forcing function in (6) during the active phase of the LG neuron.

The term I_s on the right-hand side of (2) models the slow excitatory synapse from MCN1 to the LG neuron. Physiologically, this synapse occurs within the STG (Figure 2(B.1)). The parameters $\bar{g}_s$ and E_s represent its maximal conductance and reversal potential, respectively, and the state variable s is governed by (4). The slow dynamics of s are gated by V_L due to LG presynaptic inhibition of MCN1 in the STG (Figure 2(B.1)): s approaches 1 with time constant τ_{LO} when V_L is below the voltage threshold v_{thresh} for presynaptic inhibition, and decays to 0 with time constant τ_{HI} when V_L is greater than v_{thresh}.

The buildup and decay of MCN1 input to the LG neuron is a determinant of the frequency of the gastric mill rhythm [14, 32], and the MCN1 to LG synapse operates on a much slower time scale than all other synapses in the network [14]. We account for this in our model by assigning large values to the time constants τ_{LO} and τ_{HI} in (4); see Table 1.

On the right-hand side of (2), the term $I_{C\to L}$ represents the chemical synaptic excitation from CPN2 to LG, whereas I_{elec} represents the electrical coupling between the CPN2 axon terminals and LG. Both terms model the excitation of LG by CPN2 within the STG of the biological system. In our results section, we will assume that only one of these terms is nonzero. The gating function of $I_{C\to L}$ is given by (5), and the parameters $\bar{g}_{C\to L}$ and $E_{C\to L}$ represent its maximal conductance and reversal potential, respectively. The conductance of the I_{elec} term is given by the parameter g_{elec}.

Figure 2(A) shows the evolution over time of the state variables V_I, V_L, V_C and s in the 4-dimensional model of (1)–(4). Notice that the state variable V_I oscillates in antiphase with V_L, while the state variable V_C oscillates in phase with V_L in our model.

2.2. Reduction to a 3-dimensional model of the MCN1+CPN2-elicited gastric mill rhythm. To reduce our model down to three dimensions, we absorb V_I into the LG neuron membrane potential V_L. To do so, we note that, unlike the LG neuron, Int1 is not influenced by the slow synaptic input s but only by synaptic inputs that occur on a fast time scale.

Mathematically, we divide through (1) by $g_{Leak,I}$ to get

$$\tau_I \frac{dV_I}{dt} = -\left(V_I - E_{Leak,I}\right) - \frac{\bar{g}_{L\to I}}{g_{Leak,I}} m_{L\to I}\left(V_L\right)\left(V_I - E_{L\to I}\right) - \frac{\bar{g}_P}{g_{Leak,I}} P\left(t, V_L\right)\left(V_I - E_P\right), \tag{9}$$

where $\tau_I = \frac{C_I}{g_{Leak,I}}$ is the time constant of Int1. We note that $\tau_I \ll \tau_{LO}, \tau_{HI}$ (see Table 1). Thus, we assume that V_I adjusts instantaneously to its steady state by setting $\tau_I = 0$, which makes the left-hand side of (9) equal to zero. This allows for the explicit expression of V_I in terms of the state variable V_L and the periodic forcing function $P(t, V_L)$:

$$V_I = v_I\left(V_L; P\left(t, V_L\right)\right) = \frac{g_{Leak,I} E_{Leak,I} + \bar{g}_{L\to I} m_{L\to I}\left(V_L\right) E_{L\to I} + \bar{g}_P P\left(t, V_L\right) E_P}{g_{Leak,I} + \bar{g}_{L\to I} m_{L\to I}\left(V_L\right) + \bar{g}_P P\left(t, V_L\right)}. \tag{10}$$

Substituting the expression for V_I given by (10) into the gating functions $m_{I\to L}(V_I)$ of (2) and $m_{I\to C}(V_I)$ of (3) gives a 3-dimensional model of the MCN1+CPN2-elicited gastric mill rhythm:

$$\begin{aligned} C_L \frac{dV_L}{dt} = &- \underbrace{g_{Leak,L}\left(V_L - E_{Leak,L}\right)}_{I_{Leak,L}} - \underbrace{\bar{g}_{I\to L} m_{I\to L}\left(v_I\left(V_L; P\left(t, V_L\right)\right)\right)\left(V_L - E_{I\to L}\right)}_{I_{I\to L}} \\ &- \underbrace{\bar{g}_s s\left(V_L - E_s\right)}_{I_s} - \underbrace{\bar{g}_{C\to L} m_{C\to L}\left(V_C\right)\left(V_L - E_{C\to L}\right)}_{I_{C\to L}} - \underbrace{g_{elec}\left(V_L - V_C\right)}_{I_{elec}}, \end{aligned} \tag{11}$$

$$C_C \frac{dV_C}{dt} = - \underbrace{g_{Leak,C}\left(V_C - E_{Leak,C}\right)}_{I_{Leak,C}} - \underbrace{\bar{g}_{I\to C} m_{I\to C}\left(v_I\left(V_L; P\left(t, V_L\right)\right)\right)\left(V_C - E_{I\to C}\right)}_{I_{I\to C}}, \tag{12}$$

$$\frac{ds}{dt} = \begin{cases} \dfrac{1-s}{\tau_{LO}}, & V_L \le v_{thresh}, \\ \dfrac{-s}{\tau_{HI}}, & V_L > v_{thresh}. \end{cases} \tag{13}$$

By reducing our model to 3 dimensions, we have expressed the dynamics of V_I in terms of the state variable V_L in our equations. In addition, the effects of the fast inhibitory synapses onto Int1 (which are LG inhibition of Int1 and the pyloric-timed AB inhibition of Int1; see Figure 2(B.2)) are now included into the synapses that emanate from Int1. Mathematically, the synaptic inputs onto Int1 are now included in $m_{I\to L}\left(v_I\left(V_L; P(t,V_L)\right)\right)$ for the Int1 to LG synapse in (11) and $m_{I\to C}\left(v_I\left(V_L; P(t,V_L)\right)\right)$ for the Int1 to CPN2 feedback synapse in (12). Note that the evolution of the state variables V_L, V_C, and s is practically identical to that of the 4-dimensional model in Figure 2(A).

2.3. Reduction to a 2-dimensional model of the MCN1+CPN2-elicited gastric mill rhythm. We now further reduce our model to 2 dimensions by mathematically absorbing V_C, the membrane potential of CPN2, into the membrane potential of the LG neuron. CPN2 is only influenced by the inhibitory feedback synapse from Int1 (Figure 2(B.3)), and this synapse acts with a much faster time scale than that of s, the slow MCN1 input to LG. Thus, we can again use the difference in synaptic time scales to further reduce the dimension of our model.

To carry out this reduction, we divide through (12) by $g_{Leak,C}$ to get

$$\tau_C \frac{dV_C}{dt} = -\left(V_C - E_{Leak,C}\right) - \frac{\bar{g}_{I\to C}}{g_{Leak,C}} m_{I\to C}\left(v_I\left(V_L; P\left(t,V_L\right)\right)\right)\left(V_C - E_{I\to C}\right), \tag{14}$$

where $\tau_C = \frac{C_C}{g_{Leak,C}}$ is the time constant of CPN2. As in the previous reduction, $\tau_C \ll \tau_{LO}, \tau_{HI}$ (see Table 1). Therefore, we make the simplifying assumption that V_C also adjusts instantaneously to its steady state by setting $\tau_C = 0$ to make the left-hand side of (14) equal to zero. This allows for an explicit solution of V_C in terms of the state variable V_L and the periodic forcing function $P(t, V_L)$:

$$V_C = v_C\left(v_I\left(V_L; P\left(t,V_L\right)\right)\right) = \frac{g_{Leak,C}E_{Leak,C} + \bar{g}_{I\to C} m_{I\to C}\left(v_I\left(V_L; P\left(t,V_L\right)\right)\right) E_{I\to C}}{g_{Leak,C} + \bar{g}_{I\to C} m_{I\to C}\left(v_I\left(V_L; P\left(t,V_L\right)\right)\right)}. \tag{15}$$

Substituting the expression for V_C on the right-hand side of (15) into the terms $I_{C\to L}$ and I_{elec} of (11) gives a 2-dimensional model of the MCN1+CPN2-elicited gastric mill rhythm:

$$\begin{aligned} \frac{dV_L}{dt} = &- \underbrace{g_{Leak,L}\left(V_L - E_{Leak,L}\right)}_{I_{Leak,L}} - \underbrace{\bar{g}_{I\to L} m_{I\to L}\left(v_I\left(V_L; P\left(t,V_L\right)\right)\right)\left(V_L - E_{I\to L}\right)}_{I_{I\to L}} - \underbrace{\bar{g}_s s\left(V_L - E_s\right)}_{I_s} \\ &- \underbrace{\bar{g}_{C\to L} m_{C\to L}\left(v_C\left(v_I\left(V_L; P\left(t,V_L\right)\right)\right)\right)\left(V_L - E_{C\to L}\right)}_{I_{C\to L}} - \underbrace{g_{elec}\left(V_L - v_C\left(v_I\left(V_L; P\left(t,V_L\right)\right)\right)\right)}_{I_{elec}}, \end{aligned} \tag{16}$$

$$\frac{ds}{dt} = \begin{cases} \dfrac{1-s}{\tau_{LO}}, & V_L \le v_{thresh}, \\ \dfrac{-s}{\tau_{HI}}, & V_L > v_{thresh}. \end{cases} \tag{17}$$

To simplify the notation, we will describe this system as

$$\begin{aligned} \frac{dV_L}{dt} &= -I_{Leak,L} - I_{I\to L}(p) - \bar{g}_s s\,(V_L - E_s) - I_{C\to L} - I_{elec}, \\ \frac{ds}{dt} &= \varepsilon\,(H(v_{thresh} - V_L) - s)\,/\tau_s(V_L). \end{aligned} \tag{18}$$

Here p is the periodic forcing function $P(t, V_L)$, $\varepsilon = 1/\tau_{HI}$, and

$$\tau_s(V_L) = \begin{cases} \tau_{LO}/\tau_{HI}, & V_L \le v_{thresh}, \\ 1, & V_L > v_{thresh}. \end{cases}$$

In this 2-dimensional model, the effect of the fast inhibitory feedback synapse from Int1 to CPN2 (Figure 2(B.3)) has been absorbed into the excitatory inputs from the CPN2 axon terminal to the LG neuron in (16). We did not express the CPN2 excitatory inputs, $I_{C\to L}$ and I_{elec}, in terms of p in (18) because the pyloric-timed forcing has little to no influence on them in the model. The output of the 2-dimensional model in (18) is again practically identical to the V_L and s traces of Figure 2(A) and is not replotted.

2.4. Phase plane geometry of the 2-dimensional model. The reduced 2-dimensional model in (18) can be used to analyze the network dynamics of the MCN1+CPN2-elicited gastric mill rhythm. We first compute the nullclines corresponding to the two state variables. To compute the V_L-nullcline, we note that the model is nonautonomous due to the presence of the periodic forcing p in (18). As a result, the V_L-nullcline will move in the $V_L - s$ phase plane due to the influence of the forcing function. We describe a one-parameter family of V_L-nullclines which are indexed by the values of p in the interval [0, 1]. Our expression for the family of V_L-nullclines is given by

$$s\,(V_L; p) = -\frac{I_{Leak,L} + I_{I\to L}(p) + I_{C\to L} + I_{elec}}{\bar{g}_s\,(V_L - E_s)}. \tag{19}$$

The expression in (19) describes a cubic V_L-nullcline for each p, where $p = 0$ corresponds to the unforced system (no pyloric input) and $p = 1$ corresponds to the maximally forced system (peak of the pyloric input; see Figure 3(A)). The periodic forcing shifts the V_L-nullcline back and forth between the unforced and maximally forced cubics as the value of p varies in the interval $[0, 1]$. The pyloric-timed forcing function only influences the LG neuron during its inactive phase [3, 26]; see the discussion of (6). Correspondingly, in our model, the right branch of the V_L-nullcline remains stationary in the $V_L - s$ phase plane during the active state of the LG neuron (Figure 3(A)).

For the slow state variable (s) in our model, the s-nullcline is given by the step function

$$s = H\,(v_{thresh} - V_L)\,. \tag{20}$$

Recall that v_{thresh} in (20) corresponds to the synaptic threshold voltage for LG presynaptic inhibition of MCN1. The value of v_{thresh}, chosen in the 4-dimensional model to produce oscillations, lies in the middle branch of the cubic V_L-nullcline (Figure 3(A)). If v_{thresh} is chosen so that the s-nullcline intersects one of the outer branches of the cubic V_L-nullcline,

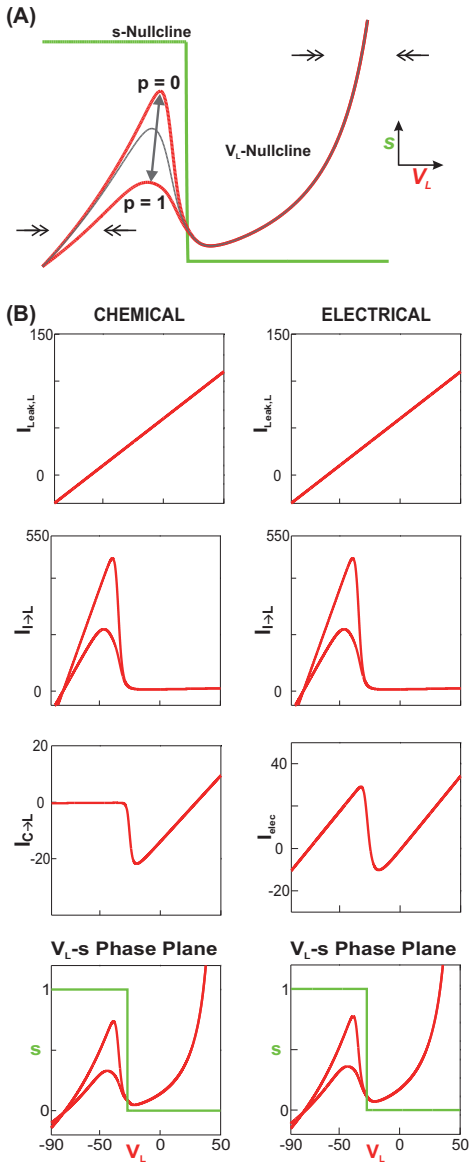

Figure 3. *Phase plane geometry of the 2-dimensional model.* (A) *The V_L- and s-nullclines intersect along the middle branch of the cubic V_L-nullcline, thus allowing for a stable limit cycle. The pyloric-timed forcing parameter p (eq. (19)) results in a family of cubic V_L-nullclines with the highest cubic ($p = 0$) corresponding to the unforced system and the lowest cubic ($p = 1$) corresponding to the maximally forced system. As p varies between 0 and 1 (double-headed arrow), the V_L-nullcline shifts between the two. Consistent with the biological system, the pyloric-timed input is inactive when LG is active, and thus the right branch of the cubic is not affected by p. The flow in the horizontal direction is shown by the double arrows.* (B) *The cubic shape of the V_L-nullcline arises from the properties of the synaptic interactions among the network neurons. The I-V relationships of the terms in the numerator of (19) illustrate how the shape of the V_L-nullcline is produced for the two alternative cases of the CPN2-to-LG synapse: chemical (left panels: $I_{C\to L}$) and electrical (right panels: I_{elec}). The terms $I_{Leak,L}$ and $I_{I\to L}$ (which depends on p) occur in both cases. The $I_{C\to L}$ and I_{elec} terms influence the V_L-nullcline differently: $I_{C\to L}$ only has an influence for high values of V_L (LG neuron active), while I_{elec} has an influence for all values of V_L. However, the overall shape of the V_L-nullcline is qualitatively similar for both cases of the CPN2-to-LG synapse (bottom panels).*

this would give rise to a globally stable fixed point and no oscillations. Regardless of the value of v_{thresh}, the flow in the horizontal direction of the $V_L - s$ phase plane is such that $dV_L/dt > 0$ above the V_L-nullcline, while $dV_L/dt < 0$ below the V_L-nullcline (Figure 3(A)). On the other hand, the flow in the vertical direction is such that $ds/dt > 0$ below the s-nullcline, while $ds/dt < 0$ above the s-nullcline.

The cubic shape of the V_L-nullcline arises from the properties of the synaptic circuitry between the network neurons and is not attributed to the intrinsic properties of any of these neurons. We now describe how this cubic nullcline is produced for the two different types of CPN2-to-LG excitation, chemical and electrical. Both cases share the terms $I_{Leak,L}$ and $I_{I\to L}$ (Figure 3(B) and (19)). For the case of the chemical CPN2-to-LG excitation, only the $I_{C\to L}$ term contributes to the shape of the V_L-nullcline (Figure 3(B), left; I_{elec} is set to zero). On the other hand, for the electrical CPN2-to-LG excitation, only the I_{elec} term contributes to the shape of the V_L-nullcline (Figure 3(B), right; $I_{C\to L}$ is set to zero). The chemical CPN2-to-LG excitation ($I_{C\to L}$) contributes to the shape of the V_L-nullcline only for higher values of V_L, which corresponds to the active phase of the LG neuron (Figure 3(B), left). In contrast, the electrical CPN2-to-LG excitation (I_{elec}) contributes to the shape of the V_L-nullcline for all values of V_L (Figure 3(B), right). The overall cubic shape of the V_L-nullcline is obtained by combining all the terms, which are present for the relevant case of the CPN2-to-LG excitation, as shown in (19). Notice that the shape of the cubic V_L-nullcline is qualitatively similar (and almost identical) for both cases, chemical and electrical, of the CPN2-to-LG excitation (Figure 3(B), bottom panels).

Because ε is small, the 2-dimensional model of (18) exists in a relaxation regime. In particular, the flow in the horizontal (V_L) direction is fast within the $V_L - s$ phase plane, while the flow in the vertical (s) direction is much slower. In the limit where $\varepsilon = 0$ and the model becomes singularly perturbed, a general trajectory in the $V_L - s$ phase plane consists of distinct fast and slow portions. In particular, the slow portions track the stable outer branches of the cubic V_L-nullcline to which they are strongly attracted by the fast, horizontal flow. On the other hand, the fast portions occur as transitions between the stable outer branches of the cubic. Previous theoretical results have established that trajectories of a relaxation (fast-slow) system for the case in which $0 < \varepsilon \ll 1$ (as occurs in (18) of our model) are closely approximated by the limiting, singularly perturbed trajectory that occurs when $\varepsilon = 0$ in the system [31]. The basic properties of the flow in the $V_L - s$ phase plane remain the same in the presence of the pyloric-timed forcing p.

All simulations for the 2-dimensional model were performed using the software package XPPAUT [18]. The graphs of the nullcline components in Figure 3(B) were produced using MATLAB. Parameter values for the intact MCN1+CPN2-elicited gastric mill rhythm are listed in Table 1. Changes in parameter values (to model the effect of changes to the circuitry of the intact system) are discussed in section 3.

3. Results. We investigate the network dynamics of the MCN1+CPN2-elicited gastric mill rhythm using a phase plane analysis of the fully reduced, 2-dimensional model in (18). The two state variables in this fully reduced model are the membrane potential of the LG neuron (V_L) and the slow, synaptic input (s) from MCN1 onto the LG neuron. As explained in section 2, we will assume that the CPN2-to-LG input in (18) is either through a chemical

excitation ($I_{C\to L}$) or through an electrical coupling (I_{elec}), and we set the other term to zero. In this section, we will focus on the case of the chemical excitation and will only discuss the electrical coupling in cases where the output is qualitatively different.

Within the $V_L - s$ phase plane, the V_L-nullcline has a cubic shape, while the s-nullcline is given by a step function (see section 2). The left branch of the cubic, V_L-nullcline corresponds to the inactive state of the LG neuron. Physiologically, during the LG inactive state (retraction phase) of the gastric mill rhythm, the LG neuron (i) is inhibited by Int1, and (ii) receives a slow, modulatory excitation (s) from MCN1. Conversely, the right branch of the cubic, V_L-nullcline corresponds to the active state of the LG neuron (protraction phase of the gastric mill rhythm). Physiologically, during this state, the LG neuron (i) inhibits Int1, (ii) presynaptically inhibits MCN1, and (iii) is excited by CPN2.

Due to the presence of the periodic forcing function p in (18), the 2-dimensional model is nonautonomous. As a result, a family of cubic V_L-nullclines (indexed by p) exists in the $V_L - s$ phase plane (Figure 3(A)). Physiologically, p models the influence of the local, inhibitory synapse from the AB neuron (the pacemaker of the pyloric network) to Int1 (see section 2).

3.1. Network dynamics without the pyloric input. We first explore the network dynamics of the MCN1+CPN2-elicited gastric mill rhythm when the local inhibitory synapse from the AB neuron to Int1 is absent ($p \equiv 0$; see schematic of Figure 4(A)). In this case, (18) becomes autonomous and only a single cubic V_L-nullcline exists in the $V_L - s$ phase plane (Figure 4(A)). Because of the fast-slow nature of the equation, the resulting trajectory of the unforced system consists of two slow and two fast portions in the phase plane. The slow portions track the stable outer branches of the V_L-nullcline, while the fast portions occur as horizontal jumps between the outer branches (Figure 4(A)). This trajectory captures the dynamics of the MCN1+CPN2-elicited gastric mill rhythm in the absence of the AB-to-Int1 synapse.

We begin on the left branch of the cubic, V_L-nullcline (Figure 4(A)). Physiologically, the left branch of the cubic corresponds to when the LG neuron is in its inactive state. Here, the slow, excitatory input s slowly builds up and, as a result, the trajectory in the $V_L - s$ phase plane slowly climbs up the left branch of the cubic (from point 1 to point 2 in Figure 4(A)). The slow buildup of s causes V_L to slowly rise (Figure 4(B)). When the trajectory reaches the left knee of the cubic at point 2, it jumps to the right branch at point 3, because the flow obeys $dV_L/dt > 0$ above the V_L-nullcline (Figure 3(A)). Physiologically, the LG neuron begins to inhibit Int1 as s slowly increases up the left branch of the cubic.

The jump to the right branch of the V_L-nullcline corresponds to when the slow buildup of s is sufficient to allow the LG neuron to escape from Int1 inhibition. As a result, the LG neuron transitions to its active state, where it inhibits Int1. LG inhibition of Int1 releases CPN2 from Int1 inhibition; as a result, CPN2 transitions to its active state, where it excites the LG neuron (red dotted trace in Figure 4(B)). Moreover, while the trajectory is on the right branch of the cubic, the LG neuron presynaptically inhibits MCN1, which causes the state variable s to slowly decay (Figure 4(B)). As a result, the trajectory slowly moves down the right branch of the cubic from point 3 to point 4 (Figure 4(A)), and V_L slowly falls as s decays (Figure 4(B)). When the trajectory reaches the right knee of the cubic at point 4, it jumps back to the left branch at point 1 (Figure 4(A)), because $dV_L/dt < 0$ below the V_L-nullcline. Physiologically, LG inhibition of Int1 decreases with V_L and s as the trajectory

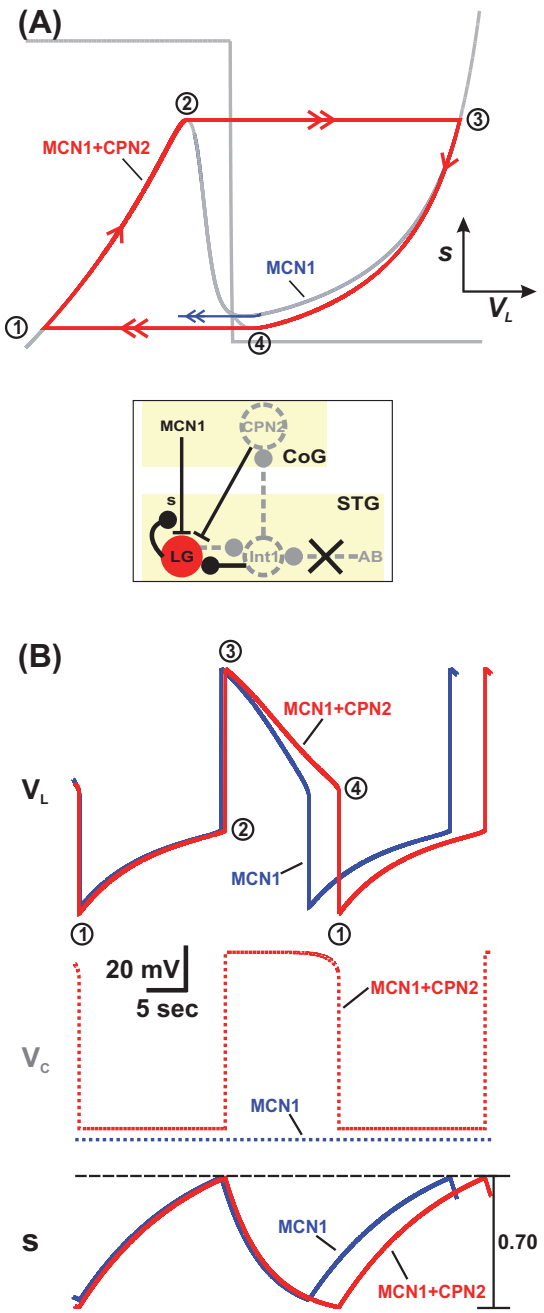

Figure 4. *The MCN1+CPN2- and MCN1-elicited gastric mill rhythms in the absence of the pyloric-timed input p. Inset shows the circuit diagram.* (A) *Phase plane diagram of the 2-dimensional model with p set to* 0. *The V_L- and s-nullclines (gray) are as in Figure* 3. *The red curve shows the oscillation trajectory of the MCN1+CPN2-elicited rhythm. Points* 1–4 *are transition points in the trajectory (see text). The V_L-nullcline for the MCN1-elicited rhythm has a distinct right branch: the blue curve shows the distinct trajectory of the MCN1-elicited gastric mill rhythm on the right knee.* (B) *Activity traces of V_L and s for the two rhythms shown in* (A). *For the MCN1+CPN2 model, the activity of V_C (calculated from V_L) is also shown. Points* 1–4 *correspond to the points in panel* A. *Dashed horizontal line in the s trace indicates that in both rhythms s reaches the same maximum value at the transition from point* 2 *to point* 3.

slowly falls down the right branch of the cubic.

The jump back to the left branch of the V_L-nullcline corresponds to when the fall in V_L is sufficient to release Int1. As a result, Int1 inhibition pushes the LG neuron (and CPN2) back down to its inactive state. In turn, LG presynaptic inhibition of MCN1 is removed, s begins to slowly build up, and the cycle repeats.

3.1.1. Comparison of the MCN1+CPN2- and MCN1-elicited gastric mill rhythms. We use Figure 4 to compare how the MCN1+CPN2-elicited gastric mill rhythm (red traces) in the absence of pyloric-timed input differs from the MCN1-elicited rhythm (blue traces) in which CPN2 is inactive. The MCN1-elicited rhythm is obtained by setting $E_{Leak,C}$ (the resting potential of CPN2) to -80 mV to reproduce the fact that CPN2 is quiescent for this version of the gastric mill rhythm in the biological system. As seen in the figure, the primary difference between the two oscillations, in this case, is that the cycle frequency of the MCN1+CPN2-elicited gastric mill rhythm is slower than that of the MCN1-elicited rhythm, whose activity we have previously described in a modeling study [26].

When the trajectory jumps to the right branch of the cubic (from point 2 to point 3), the LG neuron enters its active state, and CPN2 is released from Int1 inhibition. However, V_C jumps to a high value only for the MCN1+CPN2-elicited rhythm (and only in this case CPN2 excites LG). Thus, the jump to the right branch of the cubic enables CPN2 to excite the LG neuron and prolong the duration of its active phase (compare the two V_L traces in Figure 4(B)). Consequently, s must decay to a lower minimum value for the MCN1+CPN2-elicited gastric mill rhythm (compare the two s traces in Figure 4(B)) before the LG neuron can transition back to its inactive state (from point 4 to point 1). As a result, the state variable V_L exhibits a slightly lower minimum value for the MCN1+CPN2-elicited rhythm (Figure 4(B)). Consequently, the lower minimum value of s prolongs the network oscillations (for the case when CPN2 is activated) and causes the MCN1+CPN2-elicited gastric mill rhythm to exhibit a slower cycle frequency than the MCN1-elicited rhythm (Figure 4(B)). Notice that s attains the same maximum value for both versions of the gastric mill rhythm (horizontal black dashed line in Figure 4(B)) because the jump to the right branch in Figure 4(A) occurs for the same value of s in both cases.

3.2. Network dynamics of the intact MCN1+CPN2-elicited gastric mill rhythm. We now explore the MCN1+CPN2-elicited gastric mill rhythm in the presence of the pyloric-timed input p (see schematic of Figure 5(A)), which makes the model nonautonomous (in (18)). Note that the unforced cubic in Figure 5(A) is the same as the V_L-nullcline in Figure 4(A).

As before, we begin our description of the MCN1+CPN2-elicited gastric mill rhythm on the left branch of the V_L -nullcline, when the LG neuron is in its inactive state. Physiologically, the LG neuron and CPN2 are both inhibited by Int1 during this phase of the rhythm. Moreover, s slowly builds up in the LG neuron, and the trajectory slowly climbs up the left branch of the V_L-nullcline. However, the trajectory is shifted back and forth between the unforced (higher) and maximally forced (lower) cubic nullclines due to the effect of the pyloric-timed input p (Figure 5(A)). In particular, each peak of the input p shifts the unforced cubic down to the maximally forced cubic. Physiologically, the fast, pyloric-timed transitions between the left branches of the V_L-nullcline correspond to the small-amplitude depolarizations exhibited by V_L (Figure 5(B); see also Figure 1, right). When the trajectory reaches the level of the lower

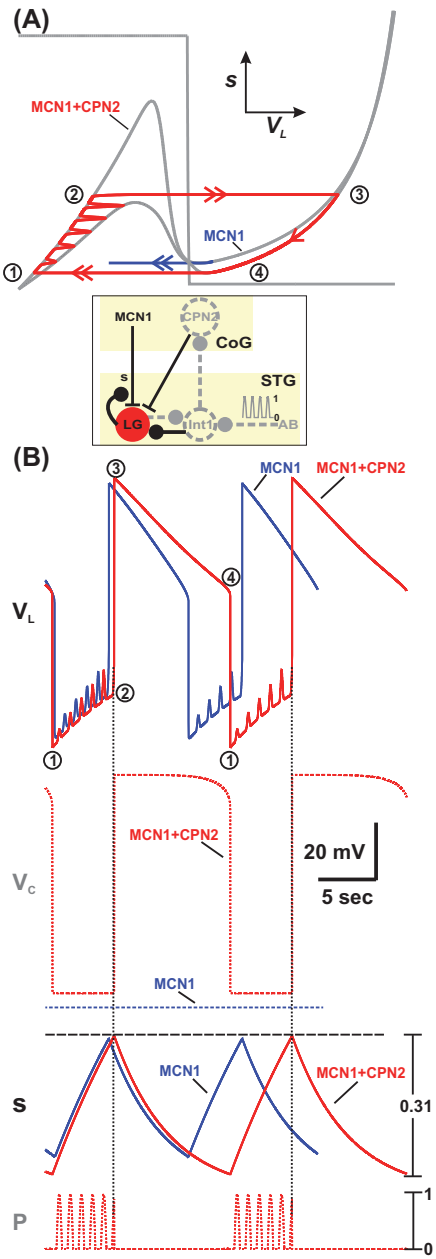

Figure 5. *The MCN1+CPN2- and MCN1-elicited gastric mill rhythms in the presence of the pyloric-timed input p. Inset shows the circuit diagram.* (A) *The phase plane showing the cubic V_L-nullcline without pyloric input ($p = 0$; upper) and with maximal pyloric input ($p = 1$; lower). The red curve shows the oscillation trajectory of the MCN1+CPN2-elicited rhythm. The trajectory shifts back and forth between the two cubic nullclines due to the pyloric-timed input. Points 1–4 are transition points in the trajectory (see text). The V_L-nullcline for the MCN1-elicited rhythm has a distinct right branch: the blue curve shows the distinct trajectory of the MCN1-elicited gastric mill rhythm on the right knee.* (B) *Activity traces of V_L and s for the two rhythms shown in* (A). *For the MCN1+CPN2 model, the activity of V_C (calculated from V_L) is also shown. Points 1–4 are as in panel* (A). *Note that CPN2 is inactive when the trajectory is on the left branch of the V_L-nullcline. As a result, the left knees of the V_L-nullcline are the same and s rises to (approximately) the same maximum value (horizontal dashed line in* (B)*).*

left knee in the phase plane, the next input peak from p shifts the V_L-nullcline below the phase point and initiates the jump to the right branch from point 2 to point 3 (Figure 5(A)).

Physiologically, the pyloric-timed shifts between cubics in the phase plane correspond to the fact that AB inhibition of Int1 in turn disrupts the Int1-to-LG inhibitory synapse in the network (see schematic of Figure 5(A)). As a result, the LG neuron is disinhibited by each forcing peak, and it exhibits the small pyloric-timed depolarizations during its inactive state (Figures 5(B) and 1). Note that the jump to the right branch of the V_L-nullcline can only occur after the trajectory reaches the level of the lower (maximally forced) left knee. Physiologically, this means that a sufficient buildup of MCN1 excitation s must first occur before the LG neuron can jump to its active state. Therefore, the trajectory cannot jump to the right branch during the first few pyloric-timed shifts. Additionally, the transition of the LG neuron to its active state coincides with a pyloric-timed forcing peak (vertical black dotted line in Figure 5(B)). Physiologically, this means that the onset of the LG active phase of the rhythm is initiated by the AB-to-Int1 inhibitory synapse. A similar effect has been established for the MCN1-elicited rhythm in previous experiments [3] and modeling [32].

After the trajectory jumps to the right branch of the V_L-nullcline, where the LG neuron enters its active state, the network dynamics are similar to that of the unforced system in Figure 4. Figure 5 also illustrates that, similar to the case of the unforced system, the MCN1+CPN2-elicited gastric mill rhythm exhibits a slower cycle frequency than the MCN1-elicited rhythm when the pyloric-timed input p is present (Figure 5(B)). This is again due to the influence of the CPN2 excitation of LG. In particular, s must decay to a lower minimum value, which prolongs the cycle period of the MCN1+CPN2-elicited gastric mill rhythm compared to that of the MCN1-elicited rhythm. Thus, the CPN2 synaptic interactions have a similar influence on the cycle frequency of the MCN1+CPN2-elicited rhythm for both the unforced (Figure 4) and intact (Figure 5) systems.

Figure 6 summarizes how the AB-to-Int1 synapse influences the MCN1+CPN2-elicited gastric mill rhythm. First, as mentioned above, this synapse initiates the onset of the LG active phase (see vertical dotted line in Figure 6(B)). This is also illustrated in the phase plane by the fact that the jump to the right branch of the V_L -nullcline is initiated by the pyloric-timed input p (red trajectory in Figure 6(A)). A second effect of the AB-to-Int1 synapse is that it increases the cycle frequency of the MCN1+CPN2-elicited gastric mill rhythm (compare red and blue in Figure 6(B)). This occurs because, in the presence of the input p, the jump to the right branch of the V_L-nullcline occurs below the higher left knee of the unforced cubic. In contrast, this jump to the right branch occurs at the higher left knee when the pyloric-timed input p is removed from the system. As a result, the duration of the trajectory on the left branch of the V_L-nullcline is reduced when the input p is present in the system. In turn, the duration of the trajectory on the right branch is also reduced because it begins at a lower point (on the right branch) in the presence of the input p (compare red and blue in Figure 6(A)). Because the right branch of the V_L-nullcline is not influenced by p, the right knee of the V_L-nullcline is the same for both cases. As a result, V_L and s decay to the same minimum values in both the unforced and intact systems (red and blue, respectively, in Figure 6(B)). We also note that previous experiments [3] and modeling [32] have shown that the AB-to-Int1 synapse has a similar influence on the MCN1-elicited rhythm.

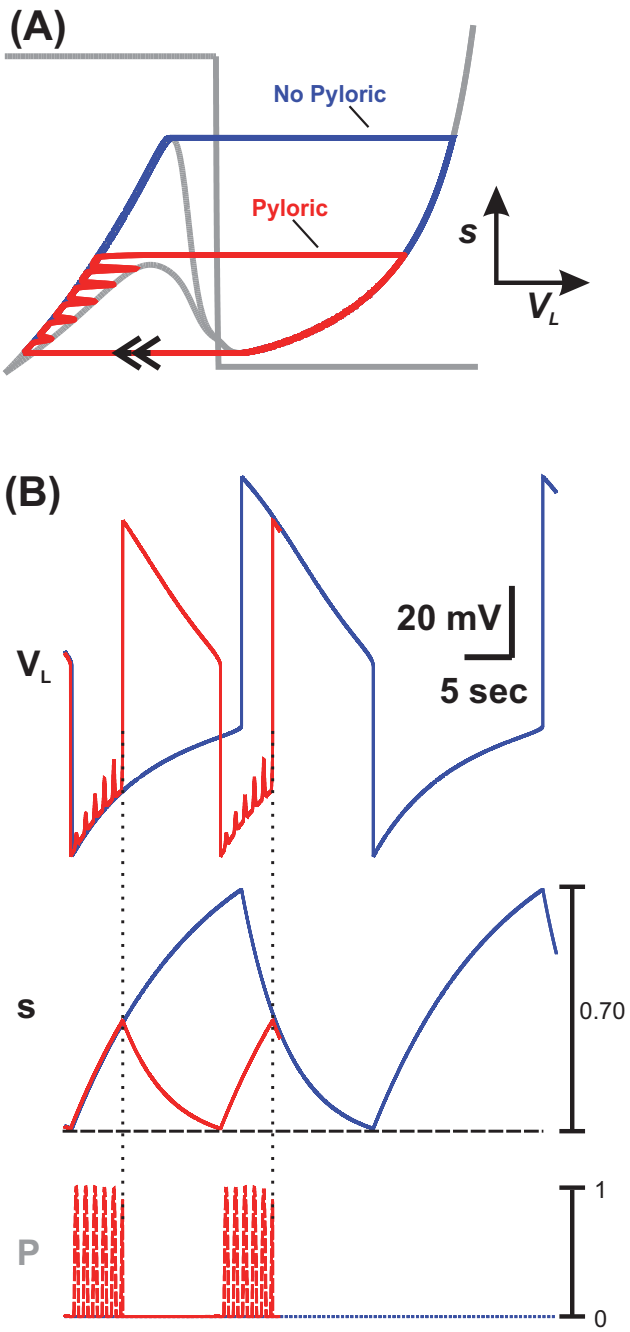

Figure 6. *The influence of the pyloric-timed input p on the MCN1+CPN2-elicited gastric mill rhythm. Red: p present; blue: p set to* 0. (A) *Phase plane diagrams.* (B) *Activity traces of V_L and s. The pyloric-timed input initiates the jump to the right branch of the V_L-nullcline (panel* (A)*) below the higher left knee of the unforced cubic. This corresponds to the jump of V_L to the active phase (vertical dotted line in* (B)*). The pyloric-timed input does not influence the right branch of the V_L-nullcline, so the right knees of this nullcline are in the same position for both cases. As a result, the transition back to the left branch of the V_L-nullcline occurs at the same value of s for both cases (horizontal dashed line in* (B)*).*

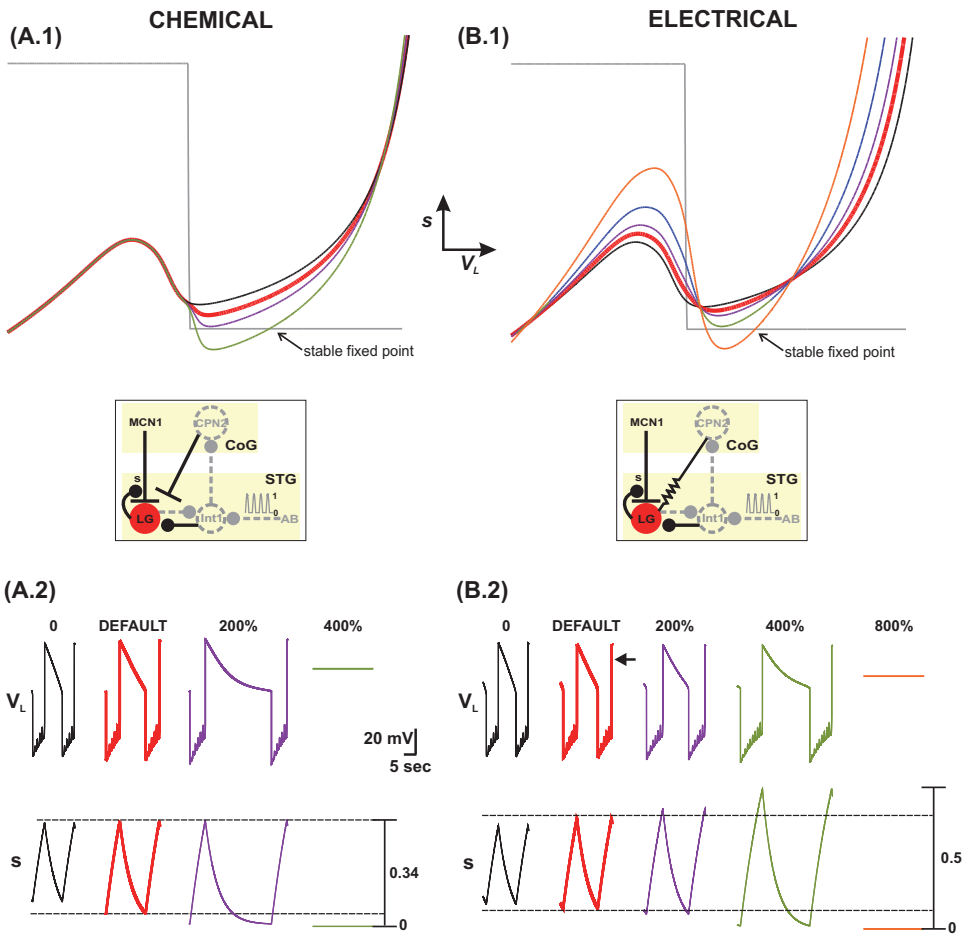

Figure 7. *Effect of strengthening the CPN2-to-LG synaptic input on the MCN1+CPN2-elicited gastric mill rhythm. For simplicity, only the $p = 1$ (maximally forced) nullcline is shown in the phase planes.* (A.1)–(A.2) *The CPN2-to-LG input modeled as an excitatory chemical synapse $I_{C\to L}$. Default V_L-nullcline is in red; zero synaptic strength in black; purple and green are* 200% *and* 400% *of default, respectively. Increasing $I_{C\to L}$ primarily influences the network for higher values of V_L by pulling down the right knee of the cubic (in* (A.1)*) so that s decays to a lower minimum value (bottom dashed line in* (A.2)*). Subsequently, the cycle period of the gastric mill rhythm is prolonged* (A.2)*. $I_{C\to L}$ has no influence on the left knee of the V_L-nullcline, so the maximum value of s remains similar in all cases where oscillations occur (top dashed line in* (A.2)*).* (B.1)–(B.2) *The CPN2-to-LG input modeled by an electrical coupling I_{elec}. Orange is the case where I_{elec} is at* 800% *of default; the other colors are as in panel* (A)*. I_{elec} influences the network for all values of V_L; thus, both knees of the V_L-nullcline move as its strength is varied. I_{elec} has an inhibitory effect when V_L is low, and therefore strengthening I_{elec} moves up the left knee of the V_L-nullcline. This gives a higher maximum value for s (top dashed line in* (B.2)*), which prolongs the LG inactive phase. When the trajectory first reaches the right branch, V_C (black arrow in* (B.2)*) is initially lower than V_L; therefore, the electrical coupling still has an inhibitory effect and a stronger I_{elec} pushes up the V_L-nullcline. All V_L-nullclines intersect at $V_L = V_C$ (in* (B.1)*). Below this intersection point, $V_C > V_L$ and I_{elec} is excitatory: a stronger I_{elec} moves down the right knee of the V_L-nullcline.*

3.3. The effect of CPN2 on the network oscillations. We now examine how the excitatory input from CPN2 to the LG neuron influences the MCN1+CPN2-elicited gastric mill rhythm. In this section we will also compare the difference between the two cases where the input from CPN2 to LG is a chemical excitation (schematic in Figure 7(A.1)) versus an electrical coupling (schematic in Figure 7(B.1)).

The chemical excitation of the LG neuron by CPN2 is modeled by $I_{C\to L}$ in (18). In the absence of this excitation, the MCN1+CPN2-elicited gastric mill rhythm reverts to the MCN1-elicited gastric mill rhythm as described above. As the maximal conductance of this synapse ($\bar{g}_{C\to L}$) is increased, the right branch of the V_L-nullcline is lowered (the $p = 1$ nullclines are shown in Figure 7(A.1)), and therefore s has to decay to a lower minimum value before the trajectory can jump back to the left branch (Figures 7(A.1) and 7(A.2)): the case in which $\bar{g}_{C\to L}$ is increased to 200% of its default value. A consequence of this is that the cycle period is increased because the LG active phase and, therefore, its inactive phase are prolonged. This can be seen, for example, by comparing the s traces below the lower dashed line for the 200% case with the default traces in Figure 7(A.2): in the 200% case, the s trace must spend an additional time interval below the dashed line compared to the default case. If $\bar{g}_{C\to L}$ is sufficiently large, the oscillations are completely disrupted (400% case in Figure 7(A.2)). This happens because a stable fixed point appears in the right branch of the V_L-nullcline (Figure 7(A.1)), causing V_L to be stuck in a depolarized state. Physiologically, this would correspond to the LG neuron being tonically active.

We now deal with the case of electrical coupling between CPN2 and the LG neuron. The electrical coupling is governed by the term I_{elec} in (18). As with the chemical excitation, the cycle period of the MCN1+CPN2-elicited gastric mill rhythm slows down and is eventually disrupted when the strength of the electrical coupling is increased in the model (Figure 7(B.2)).

First, we examine how removing the electrical coupling (by setting $g_{elec} = 0$) influences the network oscillations. When $g_{elec} = 0$, CPN2 has no influence on the LG neuron. In this case, V_L reaches the transition point (left knee of the V_L-nullcline) when the input s overcomes Int1 inhibition of the LG neuron. In contrast, in the presence of the electrical coupling, CPN2 sits at a low membrane potential, during the LG inactive state, and it has an inhibitory effect on the LG neuron by pulling V_L toward V_C. Therefore, in the presence of the electrical coupling, the LG neuron can only reach the transition point (left knee of the cubic) when the input s allows V_L to overcome both Int1 inhibition of LG and the inhibitory effect of CPN2 on LG through the electrical coupling. This is reflected in the phase plane by noting that, on the left branch of the cubic V_L-nullcline, the left knee of the $g_{elec} = 0$ case is lower than that of the default case (black vs. red in Figure 7(B.1)). As a result, s climbs to a lower maximum value compared to the default case (black vs. red in Figure 7(B.2)), and the LG inactive phase exhibits a slightly shorter duration when the electrical coupling is absent (compare s traces with the horizontal dashed lines, black vs. red in Figure 7(B.2)).

During the LG active phase, the right branch of the V_L-nullcline is initially more depolarized compared to the default case (black vs. red in Figure 7(B.1)). Physiologically, this occurs because V_C is still lower than V_L at the beginning of the LG active phase (arrow in red trace of Figure 7(B.2)). Thus, if $g_{elec} = 0$, the right branch of the cubic is initially more depolarized than the default case because the mechanism which pulls down on V_L has been removed from the model. There is a point on the right branch where the V_L-nullclines inter-

sect (Figure 7(B.1)). This point corresponds to $V_L = V_C$. Below this point, $V_C > V_L$, and the electrical coupling has an excitatory influence on V_L. Thus, when $g_{elec} = 0$, the right knee of the V_L-nullcline is higher than the default case (black vs. red in Figure 7(B.1)). This is because the decay of s (in the $g_{elec} = 0$ case) does not have to overcome the excitatory influence from the CPN2 electrical coupling before reaching the transition point (right knee of the cubic) to jump back to the left branch. The overall influence of the electrical coupling on the right branch is similar to that of the chemical excitation described in Figure 7(A.1). Similarly, as with the strong chemical excitation, if g_{elec} is sufficiently strong, a stable fixed point appears on the right branch and oscillations are disrupted. In our model, the disruption occurs at a higher level of increase in g_{elec} compared with the increase in $\bar{g}_{C\to L}$ (Figure 7(B.2) vs. 7(B.1)).

Note that the chemical excitation only influences the active phase of the LG neuron, whereas the electrical coupling influences both phases. This difference is, for example, seen in comparing the s traces in the two cases in Figures 7(A.2) and 7(B.2) (compare with the dashed lines).

3.4. Two distinct loci of oscillations in the network. One distinguishing factor in the circuit of the MCN1+CPN2-elicited gastric mill rhythm as compared to the MCN1-elicited rhythm is the presence of the Int1-to-CPN2 feedback synapse. This synapse inhibits CPN2, which prevents it from exciting the LG neuron. Yet, Int1 also has a direct inhibitory synapse onto the LG neuron. This brings up the question as to what these two seemingly redundant functionally inhibitory pathways accomplish. To address this question, we removed each pathway from the network and examined the behavior of the model.

First, we examine how the removal of the inhibitory feedback synapse from Int1 to CPN2 influences the MCN1+CPN2-elicited gastric mill rhythm. In our model, this feedback synapse appears in (3) as $I_{I\to C}$ with maximal conductance $\bar{g}_{I\to C}$. In the reduced model, this synapse is mathematically absorbed into the $I_{C\to L}$ and I_{elec} terms of (18).

Network oscillations persist when the Int1-to-CPN2 feedback synapse is removed from the network circuitry (Figure 8). This suggests that costimulation of MCN1 and CPN2 can produce a gastric mill rhythm in the absence of the Int1-to-CPN2 feedback synapse. Note that, in our model, when the Int1-to-CPN2 feedback synapse is removed from the network, the membrane potential of CPN2 remains fixed at its high resting potential (Figure 8(B)). As a result, CPN2 has an excitatory effect on V_L in both phases of the gastric mill rhythm. Moreover, during the inactive state of the LG neuron, the position of the left knee of the V_L-nullcline is lower than that of the case where the network circuitry is intact (Figure 8(A)). This is because, unlike the intact system, the excitation from CPN2 works together with the excitatory input s during the LG inactive phase of the rhythm. As a result, less buildup of s is needed before V_L can jump to its active state. However, as in the intact system, the jump to the right branch of the V_L-nullcline is still initiated by the pyloric-timed input p (vertical dotted line in Figure 8(B)).

The active state of the LG neuron remains mostly unchanged in the absence of the Int1-to-CPN2 feedback synapse (Figure 8(A)). In summary, there is no qualitative effect produced by removing the Int1-to-CPN2 feedback synapse on the MCN1+CPN2-elicited gastric mill rhythm.

Next, we examine how removal of the Int1-to-LG synapse influences the MCN1+CPN2-

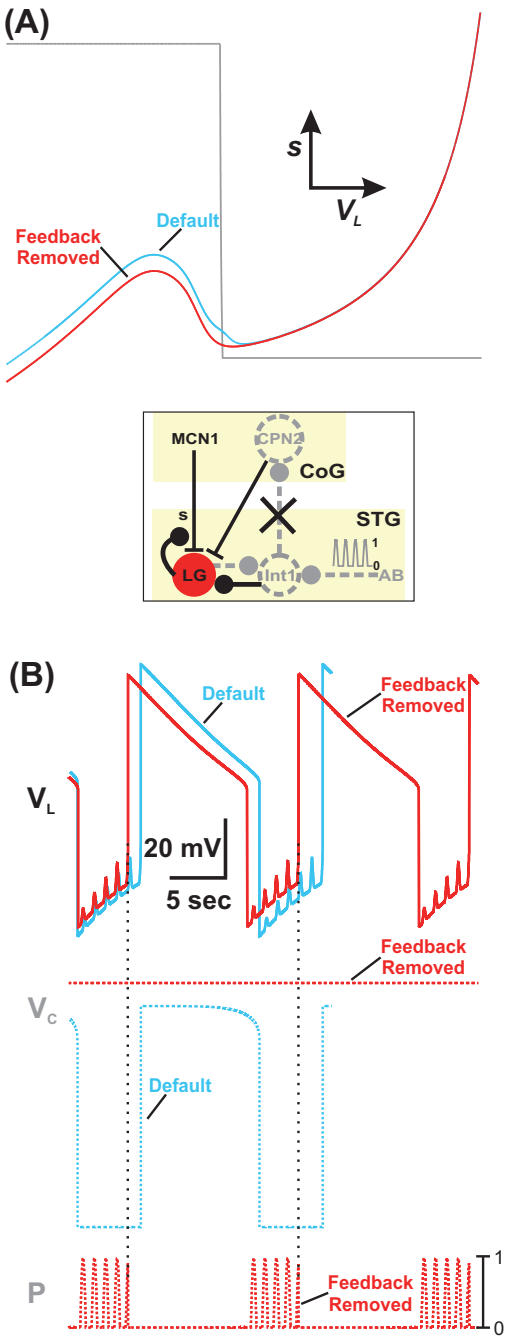

Figure 8. *Removing the Int1-to-CPN2 feedback synapse does not qualitatively change the MCN1+CPN2-elicited gastric mill rhythm. Inset shows the circuit diagram.* (A) *Phase plane diagram showing the V_L-nullcline of the intact network (default: light blue) and when the Int1-to-CPN2 feedback synapse is removed (red). For simplicity only the $p = 1$ V_L-nullcline is shown. Without the feedback synapse, V_C remains in an active state and continually excites LG. Therefore, only the left branch of the V_L-nullcline is affected by the Int1-to-CPN2 synapse.* (B) *The overall effect of removing the Int1-to-CPN2 feedback synapse is a slightly shorter cycle period. Note, however, that, similar to the intact system, the pyloric-timed input still determines the onset of the LG active phase when the Int1-to-CPN2 feedback synapse is removed (vertical dotted line).*

elicited gastric mill rhythm in the model. When this synapse is removed, the V_L-nullcline retains its cubic shape (Figure 9(A.1)), and the V_L- and s-nullclines still intersect along the middle branch of the cubic, which allows for a stable limit cycle (Figure 9(A.1)) and network oscillations persist (Figure 9(A.2)). Note that the effect of removing the Int1-to-LG synapse on the network dynamics is removal of direct inhibition of the LG neuron (schematic of Figure 9(A.1)). As a result, although the V_L-nullcline retains its cubic shape, the left knee of the V_L-nullcline is at a more depolarized value because of the absence of direct inhibition on the LG neuron (compare red and blue cubics in Figure 9(A.1)).

While the trajectory is on the left branch of the V_L-nullcline (with the Int1-to-LG synapse removed from the network), Int1 inhibits CPN2, which prevents the latter from exciting LG. Also, the MCN1 input s slowly builds up in the LG neuron (Figure 9(B.2)) as the trajectory slowly climbs up the left branch of the cubic. When the trajectory reaches the left knee of the cubic, it jumps to the LG active state on the stable right branch. Now, the LG neuron inhibits Int1 and presynaptically inhibits MCN1. The former allows CPN2 to escape from Int1 inhibition and excite the LG neuron. The latter causes s to slowly decay down the right branch of the cubic (Figure 9(A.1)). When the trajectory reaches the right knee of the cubic, it jumps back to the stable left branch, and the cycle repeats.

Note that the right branch of the cubic is practically the same with or without the Int1-to-LG synapse because this synapse has little influence when the value of V_L is large. In the absence of this synapse, the left branch of the cubic, however, is only influenced by one factor: the LG neuron leak current $I_{Leak,L}$. Figures 9(B.1) and 9(B.2) show how an increase in $g_{Leak,L}$ affects the shape of the nullcline and the network oscillations in the absence of the Int1-to-LG synapse. Note that the excitation strength for the CPN2-to-LG synapse was increased in these figures to compensate for the increase in $g_{Leak,L}$. In the case of a larger value of $g_{Leak,L}$, the left knee of the V_L-nullcline is shifted up (green cubic in Figure 9(B.1)), resulting in an increase in the inactive duration of the LG neuron oscillations (green vs. red in Figure 9(B.2)). Note also that, even with this increased $g_{Leak,L}$, oscillations persist in the intact network in the presence of the Int1-to-LG synapse (not shown).

We have shown that oscillations can persist after removing either the Int1-to-CPN2 feedback synapse or the Int1-to-LG synapse. However, removing both synapses changes the cubic V_L-nullcline to a monotonic curve, and only a single stable fixed point remains in the phase plane (Figure 9(A.1)). As a result, oscillations cannot persist without both of these synapses (Figure 9(A.2)).

In contrast with the MCN1+CPN2-elicited gastric mill rhythm, the MCN1-elicited rhythm cannot persist in the absence of the Int1-to-LG synapse. Removing this synapse disrupts the pattern-generating mechanism by changing the V_L-nullcline to a monotonic curve (not shown).

3.5. The role of the MCN1 slow input s.

As with the MCN1-elicited gastric mill rhythm [26], the slow oscillations in the MCN1+CPN2-elicited gastric mill rhythm are primarily determined by the slow rise and decay of s. The time constant of this state variable is the slow time constant in the model. In the previous section, we showed that the network circuitry underlying the MCN1+CPN2-elicited gastric mill rhythm involves two distinct loci of oscillations. Here we examine the influence of the slow input s on the gastric mill oscillations for the intact network in comparison with the oscillations that occur in the absence of the Int1-to-LG

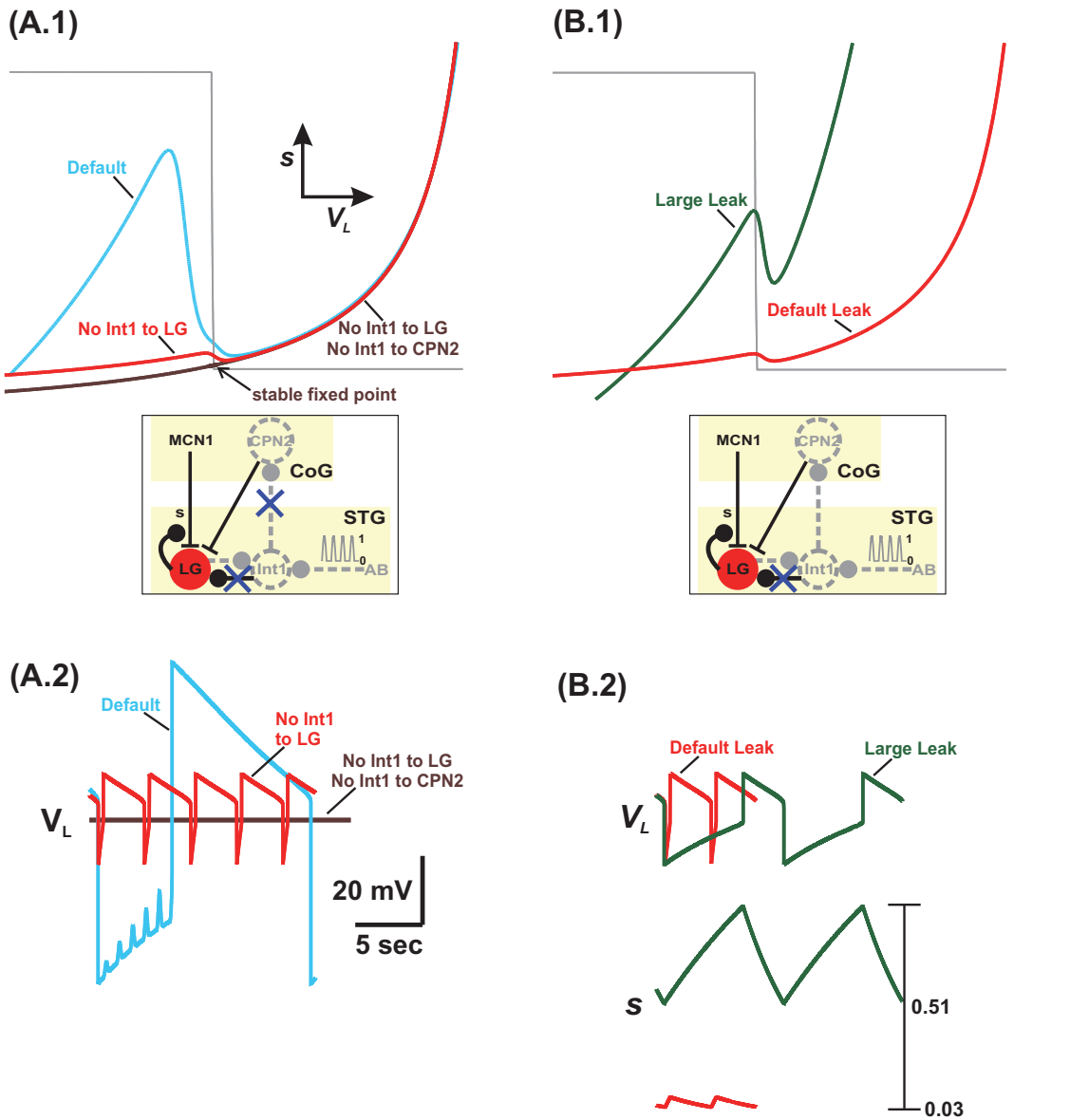

Figure 9. *The MCN1+CPN2-elicited gastric mill rhythm persists, but is qualitatively different, when the Int1-to-LG synapse is removed from the network. Inset shows the circuit diagram.* (A.1)–(A.2) *Phase plane diagram showing the V_L-nullcline of the intact network (default: light blue), when the Int1-to-LG synapse is removed (red), and when both the Int1-to-LG and Int1-to-CPN2 synapses are removed (brown). For simplicity, the $p = 0$ (unforced) V_L-nullcline is shown. Due to the much lower left knee of the red cubic in the phase plane, the cycle period of the rhythm in the absence of the Int1-to-LG synapse is much smaller than the default case (red vs. blue trace in* (A.2)*). Also, notice that the pyloric-timed input does not influence the rhythm that occurs without the Int1-to-LG synapse. Oscillations cannot occur when both synapses are removed (brown).* (B.1)–(B.2) *The LG leak current influences the cycle period in the absence of the Int1-to-LG synapse. Red shows the V_L-nullcline from panel* (A.1)*, while the green V_L-nullcline corresponds to a 10-fold increase in $g_{Leak,L}$. The stronger leak conductance shifts up the left knee of the cubic in the phase plane (green vs. red in* (B.1)*), which in turn prolongs the cycle period (green vs. red in* (B.2)*). Even with higher $g_{Leak,L}$, the pyloric-timed input does not influence the oscillations.*

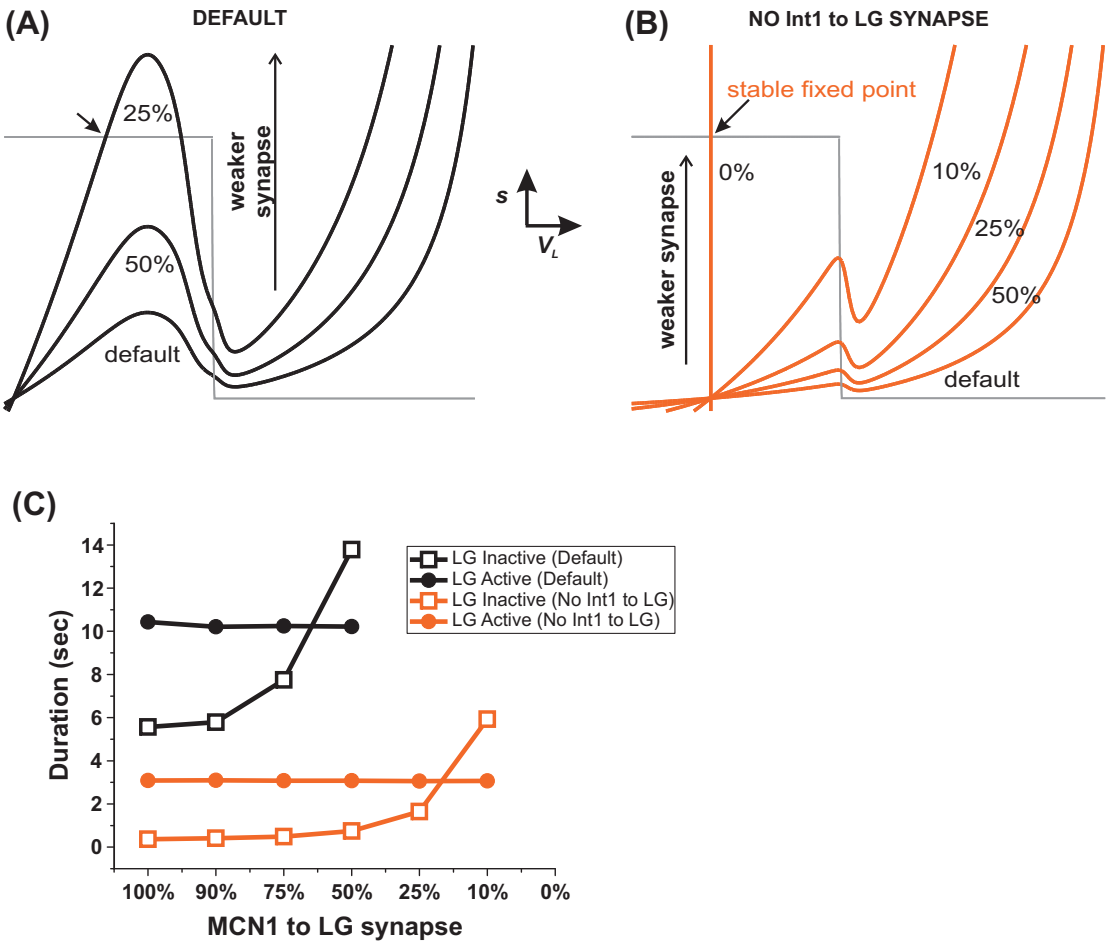

Figure 10. *Weakening the MCN1-to-LG synaptic input prolongs the duration of the LG inactive phase in the presence or absence of the Int1-to-LG synapse.* (A) *Phase plane diagram for the default case. For simplicity, only the* $p = 1$ *(maximally forced)* V_L*-nullcline is shown. Reducing* $\bar{g}_s$ *shifts up the left knee of the cubic* V_L*-nullcline. Thus, the trajectory must climb to a higher value of* s *before it can jump to the right branch. When* $\bar{g}_s$ *is weakened to* 25% *of its default value, the nullclines intersect at a stable fixed point (arrow). The right knee of the* V_L*-nullcline is not as strongly influenced by* $\bar{g}_s$*.* (B) *Phase plane diagram for the case where the Int1-to-LG synapse is removed. As in* (A)*, the left knee of the* V_L*-nullcline moves upward as* $\bar{g}_s$ *is reduced. When* $\bar{g}_s = 0$ (0%)*, the* V_L*-nullcline loses its cubic shape, and a stable fixed point appears (arrow).* (C) *The effect of reducing* $\bar{g}_s$ *on the durations of both phases of the rhythm. Both for the default case and when the Int1-to-LG synapse is removed, the LG inactive phase duration is prolonged when* $\bar{g}_s$ *is reduced. However, the LG active phase duration remains relatively unchanged.*

synapse. The influence of s on the network oscillations in the absence of the Int1-to-CPN2 feedback synapse is similar to its effects in the default case (intact network) because of the similar phase plane structure and is not separately discussed.

In the default case, the maximal conductance $\bar{g}_s$ of the MCN1-to-LG excitatory synapse influences the cycle period of the MCN1+CPN2-elicited gastric mill rhythm primarily by changing the shape of the V_L-nullcline on the left branch. The primary effect is that, with a smaller $\bar{g}_s$, the left knee of the V_L-nullcline is shifted up (Figure 10(A)). As a result, s has

to rise to a larger value before reaching this knee, thus increasing the inactive phase duration of the LG neuron. However, the duration of the active phase remains relatively unchanged. The effect of $\bar{g}_s$ on the inactive and active phase durations of the LG neuron is shown in Figure 10(C).

In the absence of the Int1-to-LG synapse, the role of s in producing the slow oscillations remains central, but the sensitivity of the oscillations to $\bar{g}_s$ is different. This is due to the fact that the V_L-nullcline is less sensitive to changes in $\bar{g}_s$ because of the lower position of the left branch of this nullcline compared to the intact system (Figure 10(B)). As seen in Figure 10(C), the inactive phase duration of the LG oscillation remains insensitive to changes in $\bar{g}_s$ up to the point that $\bar{g}_s$ is very weak (less than 25% of the default value; see Figure 10(C)). Additionally, oscillations are disrupted at a much smaller value of $\bar{g}_s$ compared to the default case.

When $\bar{g}_s$ is set to zero, the V_L-nullcline loses its cubic shape in the phase plane. As a result, the V_L- and s-nullclines intersect at a stable fixed point (Figure 10(B)), and network oscillations are disrupted. Physiologically, this implies that the MCN1 input is necessary to activate the gastric mill rhythm, and CPN2 alone cannot activate the gastric mill rhythm, consistent with previously reported experiments [34].

4. Discussion. Activity in neural networks underlying motor output is often initiated and controlled by input from descending modulatory projection pathways [13, 6, 20, 37]. In some cases, network activity that underlies similar behaviors can result from the activity of distinct sets of projection pathways [42, 16, 40]. Additionally, descending projection pathways receive feedback from their target motor networks, which can, in turn, influence the activity of the network [19, 11, 33, 43]. We are interested in the network principles that distinguish the actions of distinct projection pathways. In particular, we address the question of how feedback to the descending projection neurons can influence network activity in an oscillatory network.

We have developed a reduced mathematical model to examine how the synaptic actions of two descending projection neurons, MCN1 and CPN2, on STG neurons can produce and shape the gastric mill oscillatory motor pattern. We specifically focused on a simplified version of the gastric mill motor pattern generated by the ventral cardiac neurons in which the MCN1 input is tonically active [5]. The model included both feed-forward and feedback circuitry that exists between these projection neurons and the gastric mill CPG neurons. We specifically investigated if the synaptic circuitry alone can distinguish the two different versions of the gastric mill rhythm from each other: the version elicited by MCN1 stimulation alone [14] and the distinct version where MCN1 and CPN2 are coactive [5]. Physiologically, CPN2 is quiescent during the MCN1-elicited rhythm, so its synaptic interactions with the gastric mill CPG neurons (CPN2 excitation of LG and Int1 feedback inhibition of CPN2) influence rhythm generation in only the MCN1+CPN2-elicited gastric mill rhythm. To simplify our mathematical analysis, we reduced our model down to 2 dimensions by (i) ignoring the action potential activity and modeling only the envelopes of the bursting activity patterns, (ii) treating all neurons in the model as passive, and (iii) exploiting the difference in synaptic time scales which are present in the biological system. This reduction of dimension allowed us to capture the fast-slow network dynamics of the model in the $V_L - s$ phase plane and readily compare both versions of the gastric mill rhythm.

4.1. The network circuitry can explain the different oscillation frequencies of the distinct gastric mill rhythms. Our modeling revealed that the synaptic circuitry between the projection neurons and gastric mill CPG neurons is sufficient to explain the different oscillation frequencies exhibited in the two distinct versions of the gastric mill rhythm, and that the intrinsic properties of individual neurons do not play a central role. In our model, the MCN1+CPN2-elicited gastric mill rhythm exhibited a longer cycle period than the MCN1-elicited rhythm. This difference in cycle period occurred in both the absence (Figure 4) and presence (Figure 5) of the pyloric-timed input from the AB neuron to Int1. In both cases, CPN2 excitation of the LG neuron, which occurs during the protraction (LG active) phase of the MCN1+CPN2-elicited rhythm, lowers the right knee of the V_L-nullcline in the phase plane (Figures 4(A) and 5(A)). Mechanistically, the excitation from CPN2 opposes the slow decay of s, the MCN1 input to the LG neuron. As a result, s must fall to a lower minimum value (for the MCN1+CPN2-elicited rhythm) before the trajectory can jump back to the left branch of the V_L-nullcline. This in turn prolongs the cycle period of the MCN1+CPN2-elicited gastric mill rhythm compared to the MCN1-elicited rhythm (where CPN2 is quiescent). Previous experiments have established the difference in cycle periods between the two distinct versions of the gastric mill rhythm in the presence of the pyloric-timed input from AB to Int1 [9]. It remains to be seen if a similar difference in cycle periods, as our model predicts, occurs in the absence of the AB-to-Int1 synapse in the biological system.

Our model also showed that the presence of the pyloric-timed input produces the same network effects in the MCN1+CPN2-elicited gastric mill rhythm, as was previously reported for the MCN1-elicited rhythm [3, 32]. In particular, the pyloric-timed input determines the onset of the LG active phase and increases the oscillatory frequency of the MCN1+CPN2-elicited gastric mill rhythm in our model (Figure 6). Thus, the gastro-pyloric coordination that exists for the MCN1-elicited rhythm is preserved when the synaptic circuitry between CPN2 and the gastric mill CPG neurons is added to the network. The effect of the pyloric-timed input on the cycle frequency of the MCN1+CPN2-elicited rhythm in our model is consistent with that observed for the VCN-elicited rhythm in the biological system [42]. However, it remains to be seen if our model prediction that the pyloric-timed input determines the onset of the LG active phase (for the MCN1+CPN2-elicited rhythm) also occurs in the biological system.

A previous experimental study has indicated that the CPN2-to-LG connection is a chemical synapse [34]. However, there is also evidence that this connection may persist in a low calcium solution, indicating that at least some component of the connection is due to an electrical coupling, i.e., a gap junction between CPN2 axon terminals and the LG neuron in the STG [35]. Our model was able to reproduce the general behavior of the MCN1+CPN2-elicited gastric mill rhythm using either a chemical synapse or an electrical coupling, and the behavior of the model was mostly independent of which connection type was used. In general, the two different cases of the CPN2-to-LG synapse had a similar influence on the network oscillations. The one instance in which qualitatively different network effects were observed was in exploring the connection strengths in the model (Figure 7). Strengthening the chemical CPN2-to-LG synapse lowered only the right branch of the V_L-nullcline in the phase plane. In contrast, the electrical CPN2-to-LG coupling influenced the full V_L-nullcline. As a result, the chemical synapse has a more direct effect on the LG neuron active phase, whereas the

electrical coupling has a more symmetric effect on both the active and inactive phases of the LG neuron.

Previous experimental results have suggested that CPN2 exhibits postinhibitory rebound properties [34]. However, these intrinsic properties of CPN2 were not necessary in our model to reproduce the general behaviors of the MCN1+CPN2- and MCN1-elicited gastric mill rhythms exhibited in the biological system. It is possible to include the postinhibitory rebound properties of CPN2 in the model, but this would require a 4-dimensional model to analyze the network dynamics and would not allow for using phase plane analysis. Nevertheless, the overall behavior of network oscillations in the 4-dimensional model is similar to that of our reduced 2-dimensional model in this work [25].

An alternative possibility is that CPN2 has intrinsic bursting properties. If CPN2 is an intrinsic burster, then its influence on the MCN1+CPN2-elicited gastric mill rhythm can be quite different. As a bursting neuron, CPN2 activity can potentially dominate the gastric mill rhythm through its excitatory synapse onto the LG neuron. Thus, even in the absence of the Int1-to-CPN2 feedback synapse, the rhythm would remain mostly unchanged. However, the onset of the LG neuron active phase may not remain coordinated with the pyloric-timed input. In contrast, in our current model, removing the Int1-to-CPN2 feedback synapse diminishes the influence of CPN2 on the gastric mill rhythm, thereby resulting in a rhythm which is similar to that elicited by MCN1 alone. In addition, if CPN2 is an intrinsic burster, the role of the Int1-LG reciprocal inhibition could be greatly diminished in generating the gastric mill rhythm. In fact, CPN2 may be able to elicit a gastric mill rhythm even if all synapses from Int1 are deactivated within the network circuitry.

Previous experiments and modeling [16] have accounted for a modulator-activated, voltage-gated inward current (I_{MI}) in the LG neuron during the MCN1-elicited gastric mill rhythm. The presence of this current in a model makes the resulting MCN1-elicited rhythm quantitatively closer to that of the biological system. However, as we observed previously for the model of the MCN1-elicited rhythm [24], we found that the presence of I_{MI} does not produce a qualitatively different rhythm in our current model.

4.2. The presence of multiple loci of oscillations in the network. Reciprocal inhibition, leading to half-center oscillations, has long been established as a fundamental building block of network circuitry [29, 17, 41]. The MCN1-elicited gastric mill rhythm relies on a single reciprocally inhibitory circuit between Int1 and the LG neuron, which is necessary for producing the rhythmic activity pattern [3]. Removing either one of the Int1-LG reciprocally inhibitory synapses will disassemble the half-center and disrupt the MCN1-elicited rhythm. In our model of the MCN1+CPN2-elicited gastric mill rhythm, the Int1-LG reciprocal inhibition still plays an important role in establishing the cubic shape of the V_L-nullcline, which allows for the existence of stable oscillations. However, our model reveals an additional locus for the generation of oscillations that is independent of the Int1-LG reciprocal inhibition. As seen in Figure 9, gastric mill oscillations can persist even if the Int1-LG reciprocal inhibition is disrupted by blocking the Int1-to-LG synapse. In this case, oscillations are generated through a distinct half-center circuit which consists of three synaptic interactions: Int1 inhibition of CPN2, CPN2 excitation of LG, and LG inhibition of Int1. The first of these synaptic interactions influences the left branch of the V_L-nullcline, whereas the latter two influence the

right branch of the nullcline. Even in the absence of the Int1-to-LG inhibitory synapse, these interactions can result in a cubic V_L-nullcline and allow for stable oscillations.

Note that the oscillatory activity (in the case where the Int1-to-LG synapse is removed) is also dependent, primarily, on the slow dynamics of s, the MCN1 excitatory input to the LG neuron (Figure 9(B.2)). When CPN2 is inhibited by Int1 (and therefore LG is inactive), s slowly builds up in the LG neuron, allowing it to depolarize and eventually start inhibiting Int1. LG inhibition of Int1 results in the removal of the Int1-to-CPN2 feedback inhibition, which permits CPN2 to excite the LG neuron, thus causing a rapid transition of LG to its active state. During the LG active state, s decays due to LG presynaptic inhibition of MCN1, and the LG membrane potential decays to the point that it eventually stops inhibiting Int1, allowing the latter to escape to its active state, and the cycle repeats.

The network oscillations that occur in the absence of the Int1-to-LG synapse are distinct from the oscillations of the intact circuit. First, the cycle period is substantially shorter because LG does not need to overcome direct Int1 inhibition in order to transition to its active state. Second, the pyloric-timed input no longer influences the MCN1+CPN2-elicited gastric mill rhythm, and the gastro-pyloric intercircuit regulation is lost. Thus, this reduced network circuitry (without the Int1-to-LG synapse) does not necessarily produce a normal motor behavior as the full intact network does. Yet, there is evidence that the MCN1+CPN2-elicited gastric mill rhythm can persist in the absence of the Int1-to-LG synapse in the biological system [1]. This implies a functional role for the feedback synapse from the gastric mill CPG to the descending projection neurons, where the presence of this synapse results in a new locus of rhythm generation which can be potentially targeted by neuromodulators to regulate the network output. In general, feed-forward plus feedback circuit interactions between projection neurons and their target networks are ubiquitous in nervous systems. Therefore, it would be interesting to check if these circuit interactions can produce multiple distinct loci for the generation of oscillations in other networks as well.

4.3. Implications for sensory input to the STG. The gastropyloric muscle stretch receptors (GPRs) are sensory neurons that are activated by the stretching of the gastric mill protractor muscles in the stomach [22, 23]. Previous experiments and modeling have established that synaptic input from the GPR neurons slows the cycle frequency of the MCN1-elicited gastric mill rhythm by presynaptically inhibiting MCN1 axon terminals during the silent (interburst) phase of the LG neuron [4]. GPR presynaptic inhibition of MCN1 prolongs the duration of the LG inactive phase and leaves the duration of the LG active phase relatively unchanged, which together slows the overall cycle frequency of the MCN1-elicited gastric mill rhythm [4]. However, the influence of GPR in the biological system is phasic in that it occurs only during the LG inactive phase of the MCN1-elicited rhythm.

Our modeling results have two implications for the influence of GPR input on the gastric mill rhythm. First, when the excitatory input from MCN1 to LG was weakened in the model during both phases of the gastric mill rhythm, the result was similar to that of the phasic GPR input in the biological system: a longer cycle period in which the LG inactive phase was prolonged but the LG active phase duration remained relatively unchanged (Figure 10(C)). This suggests that a nonphasic, continuous, GPR-like input would have a qualitatively similar influence on the gastric mill rhythm. In the biological system, the excitatory MCN1 input

to the STG is already inhibited during the LG active phase of the gastric mill rhythm due to LG presynaptic inhibition of MCN1. Therefore, a further weakening of the MCN1 input should not qualitatively change the duration of the LG active phase, as confirmed by our model. Mathematically, as the MCN1 input to the LG neuron is weakened in our model, the jump to the right branch of the cubic V_L-nullcline occurs for a higher value of s. Thus, the (exponential) decay from higher values of s becomes more rapid along the right branch of the cubic as the conductance $\bar{g}_s$ is weakened in the model, which leads to a similar LG active phase duration for all cases in Figure 10(C). We note that a similar influence occurs for the MCN1-elicited rhythm due to the similar phase plane structure.

The second implication is that the influence of the GPR-like input is independent of the Int1-LG reciprocal inhibition. In particular, removing the Int1-to-LG synapse dismantles the Int1-LG reciprocally inhibitory half-center in the network; yet, the effect of weakening the MCN1-to-LG synaptic input remains qualitatively similar to that of the intact network in the model (Figure 10(C)).

4.4. Conclusions. Feedback from CPG networks to descending projection neurons is a ubiquitous but seldom understood feature of motor activity. Our simple mathematical model of the gastric mill CPG provides some clues for the potential importance of such feedback pathways. In particular, this simple model shows that the patterned activity of the feedback synapse may provide additional mechanisms for the generation of oscillatory activity that are distinct from those which are present in the isolated CPG. These additional mechanisms can have distinct dependence on network parameters and may therefore be differentially controlled by sensory or modulatory inputs. Experimental data that involve manipulation of these feedback pathways, for example, in the networks of the spinal cord, can elucidate the extent to which such mechanisms are utilized in the control of rhythmic motor activity.

REFERENCES

[1] T. Akay, D. Wood, and M. P. Nusbaum, *Reciprocal Inhibition is not necessary for generation of all gastric mill rhythms*, in Proceedings of the Society for Neuroscience 34th Annual Meeting, San Diego, CA, 2004.

[2] C. Ambrosio-Mouser, F. Nadim, and A. Bose, *The effects of varying the timing of inputs on a neural oscillator*, SIAM J. Appl. Dyn. Syst., 5 (2006), pp. 108–139.

[3] M. Bartos, Y. Manor, F. Nadim, E. Marder, and M. P. Nusbaum, *Coordination of fast and slow rhythmic neuronal circuits*, J. Neurosci., 19 (1999), pp. 6650–6660.

[4] M. P. Beenhakker, N. D. Delong, S. R. Saideman, F. Nadim, and M. P. Nusbaum, *Proprioceptor regulation of motor circuit activity by presynaptic inhibition of a modulatory projection neuron*, J. Neurosci., 25 (2005), pp. 8794–8806.

[5] M. P. Beenhakker and M. P. Nusbaum, *Mechanosensory activation of a motor circuit by coactivation of two projection neurons*, J. Neurosci., 24 (2004), pp. 6741–6750.

[6] M. C. Bellingham, *Driving respiration: The respiratory central pattern generator*, Clin. Exp. Pharmacol. Physiol., 25 (1998), pp. 847–856.

[7] D. M. Blitz, M. P. Beenhakker, and M. P. Nusbaum, *Different sensory systems share projection neurons but elicit distinct motor patterns*, J. Neurosci., 24 (2004), pp. 11381–11390.

[8] D. M. Blitz and M. P. Nusbaum, *Modulation of circuit feedback specifies motor circuit output*, J. Neurosci., 32 (2012), pp. 9182–9193.

[9] D. M. Blitz and M. P. Nusbaum, *Motor pattern selection via inhibition of parallel pathways*, J. Neurosci., 17 (1997), pp. 4965–4975.

[10] D. M. Blitz, R. S. White, S. R. Saideman, A. Cook, A. E. Christie, F. Nadim, and M. P. Nusbaum, *A newly identified extrinsic input triggers a distinct gastric mill rhythm via activation of modulatory projection neurons*, J. Exp. Biol., 211 (2008), pp. 1000–1011.

[11] J. T. Buchanan and J. F. Einum, *The spinobulbar system in lamprey*, Brain Res. Rev., 57 (2008), pp. 37–45.

[12] R. E. Burke, *The central pattern generator for locomotion in mammals*, Adv. Neurol., 87 (2001), pp. 11–24.

[13] A. Buschges, T. Akay, J. P. Gabriel, and J. Schmidt, *Organizing network action for locomotion: Insights from studying insect walking*, Brain Res. Rev., 57 (2008), pp. 162–171.

[14] M. J. Coleman, P. Meyrand, and M. P. Nusbaum, *A switch between two modes of synaptic transmission mediated by presynaptic inhibition*, Nature, 378 (1995), pp. 502–505.

[15] T. G. Deliagina, P. V. Zelenin, P. Fagerstedt, S. Grillner, and G. N. Orlovsky, *Activity of reticulospinal neurons during locomotion in the freely behaving lamprey*, J. Neurophysiol., 83 (2000), pp. 853–863.

[16] N. D. Delong, M. S. Kirby, D. M. Blitz, and M. P. Nusbaum, *Parallel regulation of a modulator-activated current via distinct dynamics underlies comodulation of motor circuit output*, J. Neurosci., 29 (2009), pp. 12355–12367.

[17] A. Doloc-Mihu and R. L. Calabrese, *A database of computational models of a half-center oscillator for analyzing how neuronal parameters influence network activity*, J. Biol. Phys., 37 (2011), pp. 263–283.

[18] B. Ermentrout, *Simulating, Analyzing, and Animating Dynamical Systems: A Guide to XPPAUT for Researchers and Students*, SIAM, Philadelphia, 2002.

[19] W. N. Frost and P. S. Katz, *Single neuron control over a complex motor program*, Proc. Natl. Acad. Sci. USA, 93 (1996), pp. 422–426.

[20] L. M. Jordan, J. Liu, P. B. Hedlund, T. Akay, and K. G. Pearson, *Descending command systems for the initiation of locomotion in mammals*, Brain Res. Rev., 57 (2008), pp. 183–191.

[21] S. Kasicki and S. Grillner, *Muller cells and other reticulospinal neurones are phasically active during fictive locomotion in the isolated nervous system of the lamprey*, Neurosci. Lett., 69 (1986), pp. 239–243.

[22] P. S. Katz, M. H. Eigg, and R. M. Harris-Warrick, *Serotonergic/cholinergic muscle receptor cells in the crab stomatogastric nervous system.* I. *Identification and characterization of the gastropyloric receptor cells*, J. Neurophysiol., 62 (1989), pp. 558–570.

[23] P. S. Katz and R. M. Harris-Warrick, *Serotonergic/cholinergic muscle receptor cells in the crab stomatogastric nervous system.* II. *Rapid nicotinic and prolonged modulatory effects on neurons in the stomatogastric ganglion*, J. Neurophysiol., 62 (1989), pp. 571–581.

[24] N. Kintos, D. F. Hsu, A. Bose, M. P. Nusbaum, and F. Nadim, *Modeling the activation of a voltage-gated ionic current by a modulatory projection neuron*, Soc. Neurosci. Abstr., Chicago, IL, 2009.

[25] N. Kintos, M. P. Nusbaum, and F. Nadim, *Feedback to descending projection neurons can override the mechanisms underlying rhythmic pattern generation in the target network: A modeling study*, Soc. Neurosci. Abstr., 33 (2007), 925.1.

[26] N. Kintos, M. P. Nusbaum, and F. Nadim, *A modeling comparison of projection neuron- and neuromodulator-elicited oscillations in a central pattern generating network*, J. Comput. Neurosci., 24 (2008), pp. 374–397.

[27] Y. Manor, F. Nadim, L. F. Abbott, and E. Marder, *Temporal dynamics of graded synaptic transmission in the lobster stomatogastric ganglion*, J. Neurosci., 17 (1997), pp. 5610–5621.

[28] Y. Manor, F. Nadim, S. Epstein, J. Ritt, E. Marder, and N. Kopell, *Network oscillations generated by balancing graded asymmetric reciprocal inhibition in passive neurons*, J. Neurosci., 19 (1999), pp. 2765–2779.

[29] E. Marder and R. L. Calabrese, *Principles of rhythmic motor pattern generation*, Physiol. Rev., 76 (1996), pp. 687–717.

[30] K. Matsuyama, F. Mori, K. Nakajima, T. Drew, M. Aoki, and S. Mori, *Locomotor role of the corticoreticular-reticulospinal-spinal interneuronal system*, Prog. Brain Res., 143 (2004), pp. 239–249.

[31] E. F. Mishchenko and N. K. Rozov, *Differential Equations with Small Parameters and Relaxation Oscillators*, Plenum Press, New York, 1980.

[32] F. Nadim, Y. Manor, M. P. Nusbaum, and E. Marder, *Frequency regulation of a slow rhythm by a fast periodic input*, J. Neurosci., 18 (1998), pp. 5053–5067.
[33] B. J. Norris, M. J. Coleman, and M. P. Nusbaum, *Pyloric motor pattern modification by a newly identified projection neuron in the crab stomatogastric nervous system*, J. Neurophysiol., 75 (1996), pp. 97–108.
[34] B. J. Norris, M. J. Coleman, and M. P. Nusbaum, *Recruitment of a projection neuron determines gastric mill motor pattern selection in the stomatogastric nervous system of the crab, Cancer borealis*, J. Neurophysiol., 72 (1994), pp. 1451–1463.
[35] M. P. Nusbaum, *Private communication*, 2014.
[36] M. P. Nusbaum and M. P. Beenhakker, *A small-systems approach to motor pattern generation*, Nature, 417 (2002), pp. 343–350.
[37] M. P. Nusbaum, D. M. Blitz, A. M. Swensen, D. Wood, and E. Marder, *The roles of co-transmission in neural network modulation*, Trends Neurosci., 24 (2001), pp. 146–154.
[38] M. C. Perreault, T. Drew, and S. Rossignol, *Activity of medullary reticulospinal neurons during fictive locomotion*, J. Neurophysiol., 69 (1993), pp. 2232–2247.
[39] S. Rossignol, R. Dubuc, and J. P. Gossard, *Dynamic sensorimotor interactions in locomotion*, Physiol. Rev., 86 (2006), pp. 89–154.
[40] W. Stein, N. D. Delong, D. E. Wood, and M. P. Nusbaum, *Divergent cotransmitter actions underlie motor pattern activation by a modulatory projection neuron*, Eur. J. Neurosci., 26 (2007), pp. 1148–1165.
[41] A. E. Tobin and R. L. Calabrese, *Endogenous and half-center bursting in morphologically inspired models of leech heart interneurons*, J. Neurophysiol., 96 (2006), pp. 2089–2106.
[42] R. S. White and M. P. Nusbaum, *The same core rhythm generator underlies different rhythmic motor patterns*, J. Neurosci., 31 (2011), pp. 11484–11494.
[43] D. E. Wood, Y. Manor, F. Nadim, and M. P. Nusbaum, *Intercircuit control via rhythmic regulation of projection neuron activity*, J. Neurosci., 24 (2004), pp. 7455–7463.
[44] T. Yamaguchi, *The central pattern generator for forelimb locomotion in the cat*, Prog. Brain Res., 143 (2004), pp. 115–122.
[45] P. V. Zelenin, *Activity of individual reticulospinal neurons during different forms of locomotion in the lamprey*, Eur. J. Neurosci., 22 (2005), pp. 2271–2282.